

<sup>1</sup>

José D. Ruiz-Álvarez

<sup>2</sup>

Compiled on 04/05/2015 at 00:41



### <sup>3</sup> Chapter 1

## <sup>4</sup> The CMS experiment at LHC

<sup>5</sup> The CMS experiment is one of the biggest particle physics experiments on the world. It  
<sup>6</sup> is located at the ring of the LHC that is the main accelerator managed by CERN, the  
<sup>7</sup> European Organization for Nuclear Research or Centre Européenne pour la Recherche  
<sup>8</sup> Nucléaire by its french name. This center constitutes the biggest center for research  
<sup>9</sup> on particle physics all over the world. All along its 60 years of existence, from 1954,  
<sup>10</sup> 21 member states have been joining it, but an overall of 113 countries participate in  
<sup>11</sup> different ways on this center.

<sup>12</sup> On the present chapter we discuss in detail different aspects of the LHC accelerator  
<sup>13</sup> and the CMS experiment. In particular we make some emphasis in the CMS sub-  
<sup>14</sup> detectors related to jets, objects that play the main role on the search that is the main  
<sup>15</sup> subject of the present work. We also discuss the present state of both machines, their  
<sup>16</sup> achievements and the challenges that were overcome. Finally, also the expectations and  
<sup>17</sup> goals for the upcoming run II are mentioned.

### <sup>18</sup> 1.1 The Large Hadron Collider

<sup>19</sup> The Large Hadron Collider, or LHC [1], is a machine that accelerates and collides protons  
<sup>20</sup> and lead. This machine is the biggest particle collider nowadays with a circumference of  
<sup>21</sup> 27 km. It also achieves the highest energy by a collider up to present, planned to be 14  
<sup>22</sup> TeV at the center of mass of the collision. On the first run of the machine only 8 TeV  
<sup>23</sup> were achieved, and next run is planned to start with 13 TeV. It's located in French-Swiss  
<sup>24</sup> border near to Geneva. The tunnel for the machine was carved around 100 m under  
<sup>25</sup> the ground, 45 m under the Jura mountains and 170 m under the Léman lake with an  
<sup>26</sup> inclination of around 1.4%, sloping down towards the lake . This machine has used as  
<sup>27</sup> much as possible old LEP buildings and sites, that was an electron-positron collider built  
<sup>28</sup> between 1984 and 1989.

<sup>29</sup> The protons and heavy ions accelerated by the machine collide in different points  
<sup>30</sup> where dedicated experiments are located to detect and study the product from the col-  
<sup>31</sup> lisions. The four main experiments located on the LHC ring are CMS [2, 3], ATLAS [4],  
<sup>32</sup> LHCb [5] and ALICE [6]. The first two are experiments of generic purpose where searches

33 for new physics and also precision measurements are performed. LHCb is dedicated to  
 34 the physics of the b-quark, and ALICE focuses on the study of the quark-gluon plasma  
 35 produced from heavy ions collisions. Even if one of the principal objectives of the con-  
 36 struction of the LHC was the search for the Higgs boson, generic searches on new physics  
 37 have been conducted from the very beginning of the first data taking in 2009. Moreover,  
 38 after the Higgs discovery in 2012 there is a growing effort on the searches for new physics  
 39 and precision measurement of the properties of the Higgs.

40 The LHC is a complex machine composed of several parts. The two principal parts  
 41 are the injector chain and the main ring. A diagram of the whole CERN complex can  
 42 be seen in figure 1.1. The injector chain has different stages that pre-accelerate protons  
 43 and heavy ions to be injected into the main ring of LHC.

#### 44 1.1.1 Injector chain

45 The injector chain begins with the proton source. Protons are extracted via ionization  
 46 of Hydrogen gas in the Duoplasmatron Proton Ion Source. Such extraction is pulsed,  
 47 what makes up the first bunch structure. The extracted protons are then accelerated up  
 48 to 50 MeV in the linear accelerator, Linac2, that dates from 1978. After this first stage  
 49 several steps are followed:

- 50 1. Linac2 injects proton bunches in the Proton Synchrotron Booster (PSB) where  
 51 they are accelerated to 1.4 GeV.
- 52 2. From PSB, the protons are delivered to the Proton Synchrotron (PS) where they  
 53 reach an energy of 25 GeV. In the PS the bunches are also split from 6 initial  
 54 bunches to 72 spaced by 25 ns.
- 55 3. Finally, the pre-acceleration chain is finished by the SPS, Super Proton Syn-  
 56 chrotron. There the bunches are accelerated up to 450 GeV right before being  
 57 inserted into the main LHC ring.

58 The whole pre-acceleration chain has been optimized to obtain the best possible  
 59 performance on the final acceleration in the LHC main ring. All parameters are carefully  
 60 controlled, for example the number of bunches, the separation between bunches, the  
 61 separation between trains of bunches or the injection energy to each subsystem. It's also  
 62 remarkable to notice the level of control achieved in the bunches manipulation, from old  
 63 subsystems as the PS from 1959 or the newest, the SPS that dates from 1976.

64 Some recent plans for future accelerator have been studied using the LHC main ring  
 65 as injector for a bigger accelerator, for example the so called FCC (Future Circular  
 66 Collider) at CERN. The FCC could be built perform proton-proton, electron-positron  
 67 or electron-proton collisions, versions that are called respectively FCC-hh, FCC-ee and  
 68 FCC-he. The FCC-hh is being designed to achieve 100 TeV of center of mass energy in  
 69 a tunnel of 80-100 km of circumference.

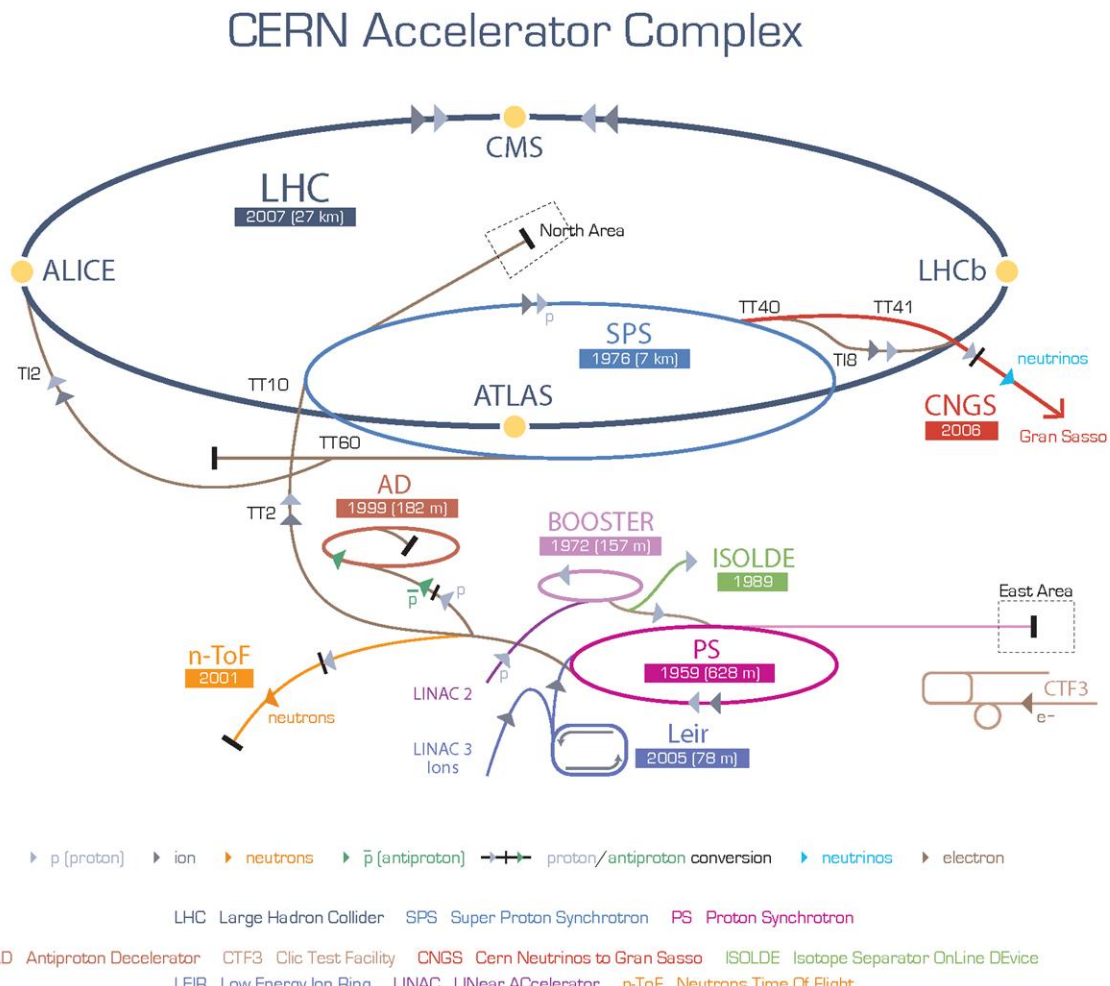


Figure 1.1: Organization of CERN accelerator complex

70 **1.1.2 Main ring**

71 The main ring is composed of two rings that accelerate the proton bunches in opposite  
 72 directions, clock-wise and counter clock-wise. An schematic view of the design of the  
 73 main ring can be seen in figure 1.2. The rings crosses in different points in order to  
 74 collide the protons and they are divided in eight straight sections and eight arcs. In each  
 75 octant bunches are controlled by dipole magnets. These complex magnets, in figure 1.3,  
 76 need to produce a very strong magnetic field in order to be able to bend a 7 TeV beam  
 77 of protons. This intense magnetic field, 8.33 T, in opposite directions, is produced by  
 78 electrical currents that are only achievable by means of superconductivity. All the 1232  
 79 dipoles operate at a temperature of 1.9 K, under cooling by liquid helium. They also  
 80 operate under ultra-high-vacuum. The beam lines with a pressure less than  $10^{-9}$  mbar  
 81 and the whole dipole system with  $10^{-6}$  mbar, that serves also as insulating system from  
 82 the surroundings. In addition, the LHC main ring has other magnets that focus and  
 83 correct different characteristics of the beam: 520 quadrupoles, 2464 sextupoles, 1232  
 84 octupoles.

85 **Luminosity**

86 In collider physics, such as the LHC, the figure of merit is the luminosity, given in  
 87 equation 1.1. The number of events per second is proportional to the luminosity, hence  
 88 is the quantity to be maximized by the design and operation of the accelerator. The  
 89 collider characteristics depend on the number of bunches in the ring  $n_b$ , the number of  
 90 protons per bunch  $N_b$ , the revolution frequency  $f_{rev}$ , the relativistic gamma factor  $\gamma$ , the  
 91 normalized rms transverse beam emittance  $\epsilon_n$  and the beta function at the interaction  
 92 point  $\beta^*$ . The denominator on 1.1 can also be rewritten in terms of the horizontal  
 93 and vertical width of the bunches at the crossing,  $\sigma_x^*$  and  $\sigma_y^*$ . In addition, there is the  
 94 geometric reduction factor ( $R$ ) that introduces a dependence on the crossing angle of the  
 95 bunches at the interaction points. In table 1.1.2 can be found the LHC beam parameters  
 96 at injection and collision.

$$L = \frac{n_b N_b^2 f_{rev} \gamma}{4\pi \epsilon_n \beta^*} R = \frac{n_b N_b^2 f_{rev}}{4\pi \sigma_x^* \sigma_y^*} R \quad (1.1)$$

| Parameter/units   | Injection | Collision             |
|---|-----------|-----------------------|
| Energy [GeV]  | 450       | 7000                  |
| Luminosity [ $\text{cm}^{-2}\text{s}^{-1}$ ]                            |           | $10^{34}$             |
| $k_b$ Number of bunches   | 2808      |                       |
| Bunch spacing [ns]  | 24.95     |                       |
| $N_b$ intensity per bunch [protons/bunch]                               |           | $1.15 \times 10^{11}$ |
| Beam current [A]  | 0.58      |                       |
| $\epsilon_n$ normalized rms transverse beam emittance [ $\mu\text{m}$ ] | 3.5       | 3.75                  |
| $f_{rev}$ revolution frequency [kHz]                                    |           | 11.25                 |

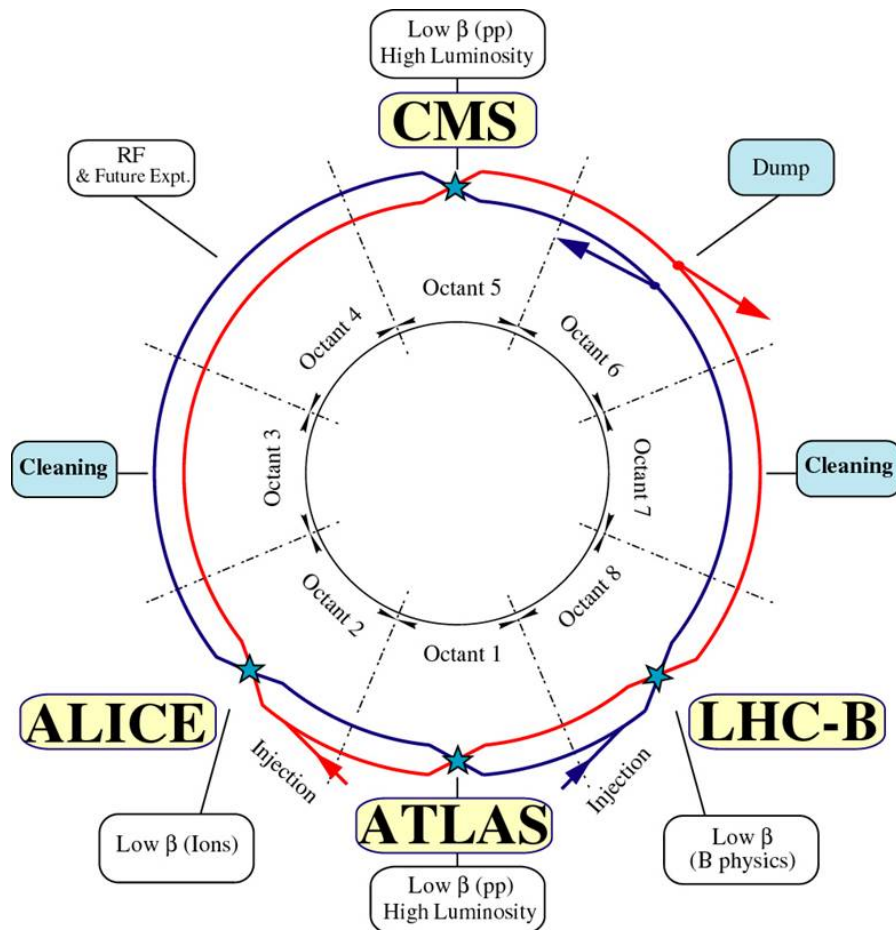


Figure 1.2: Schematic of the LHC main ring design.

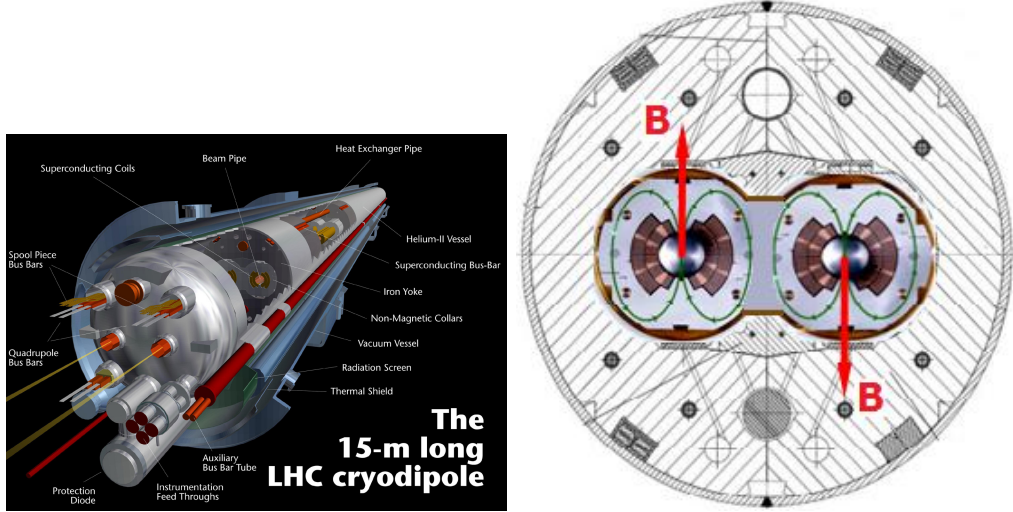


Figure 1.3: Design of LHC cryodipole and the magnetic field that bends the beam in the main ring.

97 At the crossing points, the number of events coming from collisions and produced  
 98 via a specific process, is directly proportional to the luminosity provided by the collider,  
 99 as in equation 1.1.

$$N_{events} = L\sigma_{process} \quad (1.2)$$

100 where  $\sigma_{process}$  is the cross section of the process.

101 The total cross section of a proton-proton collision from the crossing of two bunches at  
 102 14 TeV is 100-110 mb [7], from three different scattering processes: elastic, diffractive and  
 103 inelastic. In the elastic scattering the protons only exchange momenta but their structure  
 104 remain unchanged, that is the case for the majority of collisions. In diffractive scattering  
 105 momenta is exchanged and also new particles are produced in addition to the two final  
 106 protons. Finally, in inelastic scattering, the constituents of the protons, the partons,  
 107 interchange a big amount of momentum and produce a large quantity of particles. The  
 108 inelastic processes contribute less than diffraction to the total cross section. While  
 109 inelastic collisions produce particles in the central rapidity (defined in 1.2.1) region,  
 110 diffractive and elastic final products have a large rapidity. Only in the hard interactions,  
 111 inelastic scattering, color is exchanged, being the reason to fill up the central rapidity  
 112 region.

113 From the crossing of two bunches not only one proton-proton interaction is expected.  
 114 In average, 25 interactions are expected for each crossing. From them, only one is coming  
 115 from an inelastic collision, that is the type of process of more interest for detectors as  
 116 CMS or ATLAS. This fact puts an additional difficulty to the detectors in order to  
 117 extract the hard interaction from all the elastic and diffractive collisions happening at

<sup>118</sup> same time. Such phenomena is known as Pile-Up, an illustration of a collision with high  
<sup>119</sup> pile-up can be found on figure 1.4 as seen by the CMS detector.

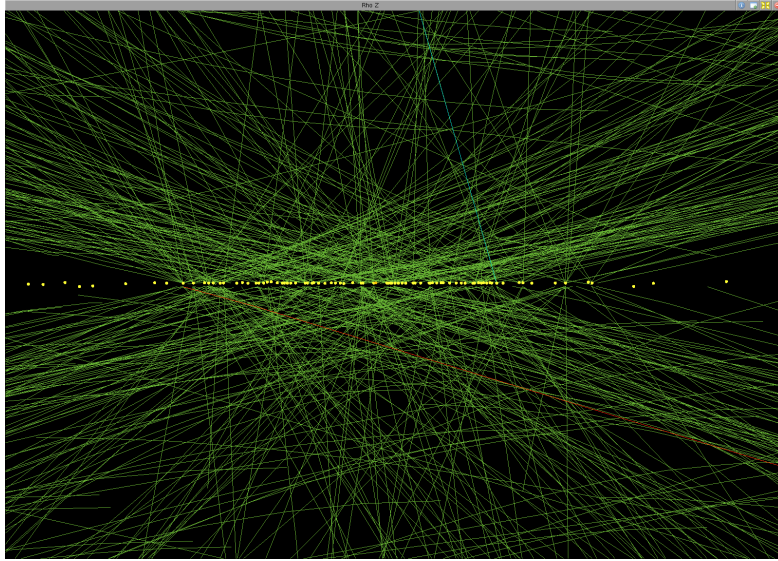


Figure 1.4: High pile-up event (78 interactions) seen by CMS detector. Event 35655522, from 198609 run, lumi 56, recorded on 2012. Image credit: Andre Holzner ©CERN

### <sup>120</sup> 1.1.3 Run 1

<sup>121</sup> On February 10 of 2013 the first stable run of the LHC reached an end. This run, now  
<sup>122</sup> called Run 1, started on November 20 of 2009. LHC was originally planned to start in  
<sup>123</sup> 2008, but an incident on one of the electric connections of one of the magnets forced to  
<sup>124</sup> stop on the 19th of September of the same year. From the restart in 2009, the energy  
<sup>125</sup> was augmented from 450 GeV to 4 TeV per beam. The 23th of September 2009 the first  
<sup>126</sup> collisions were detected by the experiments. One week after, the achieved center of mass  
<sup>127</sup> energy was  $\sqrt{s} = 2.36$  TeV, already higher than Tevatron (0.98 TeV).

<sup>128</sup> In 2010, from 30th March to 6th December 3.5 TeV per beam were reached delivering  
<sup>129</sup> near  $50 \text{ pb}^{-1}$ . With the same energy, approximately  $6 \text{ fb}^{-1}$  were delivered in 2011.

<sup>130</sup> In 2012, the center of mass energy reached one additional TeV,  $\sqrt{s} = 8$  TeV, and  
<sup>131</sup> around  $20 \text{ fb}^{-1}$  of integrated luminosity were delivered between April and December.  
<sup>132</sup> On figure 1.5 can be seen the progress of the recorded luminosity by CMS for 2010-2012  
<sup>133</sup> period. The first six weeks of 2013 were devoted to proton-lead collisions.

<sup>134</sup> After this very successful run, the LHC has been stopped for more than a year for  
<sup>135</sup> repair and maintenance of different systems in the experiments and in the LHC itself to  
<sup>136</sup> achieve higher energies. After this period, known as Long Shutdown or LS1, the LHC  
<sup>137</sup> is planned to restart a new run on the early spring of 2015.

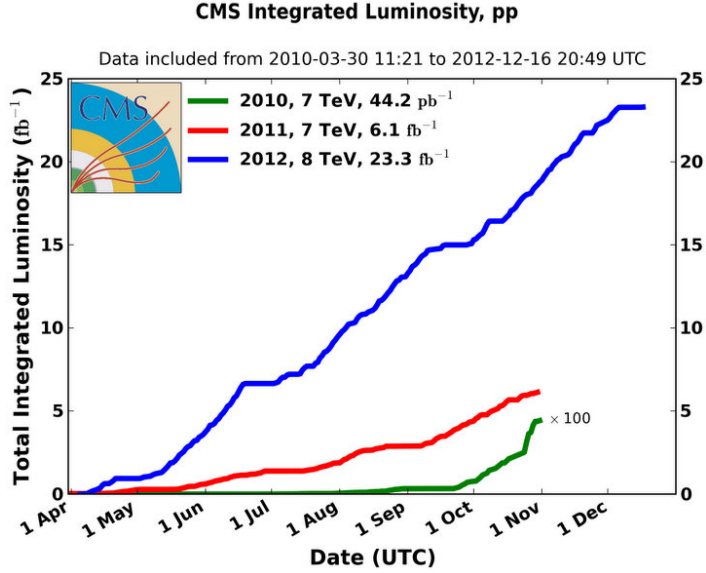


Figure 1.5: CMS integrated luminosity for proton-proton collisions delivered by LHC.  
©CERN

### 138 1.1.4 Other experiments at LHC

139 On the main ring there are several experiments depending on the collisions delivered by  
 140 the LHC main ring. The biggest are CMS [2] and ATLAS [4], both of them generalist  
 141 experiments designed to do precision measurements as well as new physics searches.  
 142 Mainly recording proton-proton collisions, they have also recorded lead-lead and proton-  
 143 lead collisions during the run 1. Both of them were designed for high instantaneous  
 144 luminosity,  $L = 10^{34} \text{ cm}^2 \text{s}^{-1}$ .

145 In addition, there are two other experiments designed for specific purposes. The  
 146 LHCb [5] that focus on the study of the physics of the b-hadrons, specially related to the  
 147 CP violation, and ALICE [6] built for the study of strongly interacting matter. The first  
 148 of them record proton-proton collisions at an instantaneous luminosity of  $10^{32} \text{ cm}^2 \text{s}^{-1}$   
 149 and the second record ion-ion collision with  $L = 10^{27} \text{ cm}^2 \text{s}^{-1}$ .

150 The CMS experiment is going to be described in detail in section 1.2. In the following  
 151 sections we are going to present very briefly the other three experiments mentioned  
 152 above.

### 153 ATLAS

154 The ATLAS experiment (A Toroidal LHC ApparatuS) is the biggest LHC experiment.  
 155 It's located at point one, as displayed on figure 1.2, on the LHC main ring. It's a  
 156 cylindrical detector similar to CMS, about 45 meter long, 25 meter high, and weights  
 157 around 7000 tons. ATLAS main components are, from inside to outside, a tracking

158 system, an electromagnetic calorimeter, a hadron calorimeter and muon chambers. In  
 159 between this subsystems there is an internal solenoidal magnet and a set of external  
 160 toroidal magnets. The detector design is presented on figure 1.6.

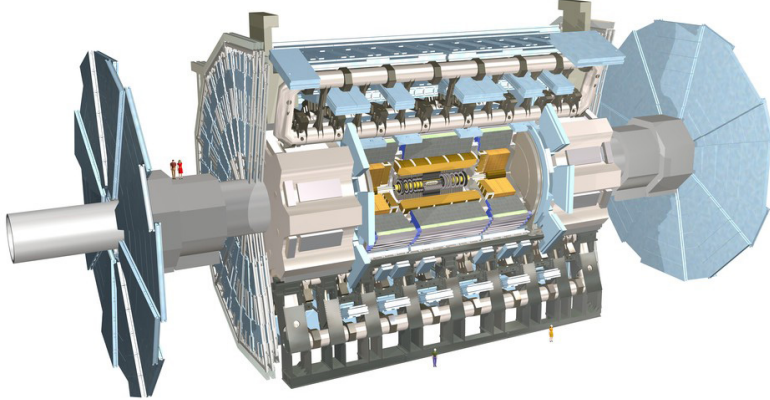


Figure 1.6: ATLAS detector internal view. ©CERN

161 On the human resources side, ATLAS experiment configures a collaboration of around  
 162 3000 persons, coming from 117 universities around the world, from 38 countries. Thirty  
 163 percent of the collaboration are students.

#### 164 **LHCb**

165 LHCb detector, hosted at point 8 of the LHC main ring, has a different design than CMS  
 166 and ATLAS. Smaller than these, its design mainly focus to be able to detect particles  
 167 produced close to the beam direction. This is the reason why it is not cylindrically but  
 168 conically shaped, in two detection arms 1.8. It also has the same main parts, a tracking  
 169 system with a very precise vertex locator, electromagnetic and hadron calorimeters,  
 170 muon chambers and magnets. Its major specificity is a system that allows to identify  
 171 different hadrons, what is crucial for the study of strong interacting matter. It measures  
 172 21 m long, 10 m high and 13 m wide, and weights 4500 tons. A view of the detector  
 173 can be found on figure 1.7. The LHCb collaboration groups around 700 persons from 50  
 174 different universities over 15 countries.

#### 175 **ALICE**

176 The ALICE experiment (A Large Ion Collider Experiment) is located at point 2 of the  
 177 LHC main ring, measures 16 m high, 16 m wide and 26 m long, and weights 10000 tons.  
 178 It's an asymmetrical detector as LHCb. Its structure can be seen on figure 1.9. ALICE  
 179 collaboration counts around 1500 people, from 154 physics institutes in 37 countries.

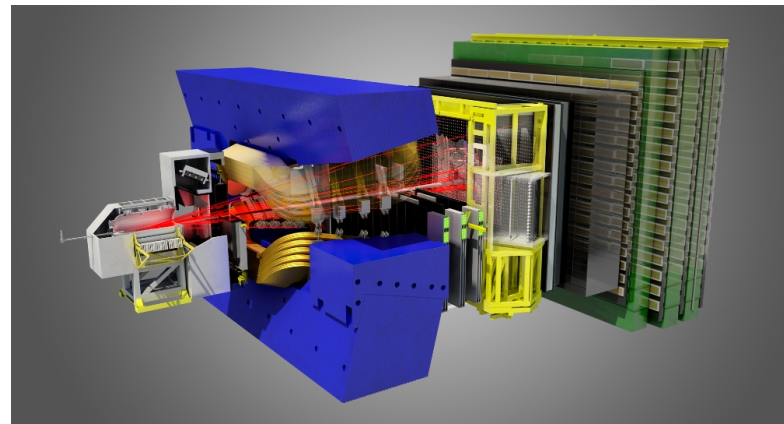


Figure 1.7: LHCb detector internal view. ©CERN

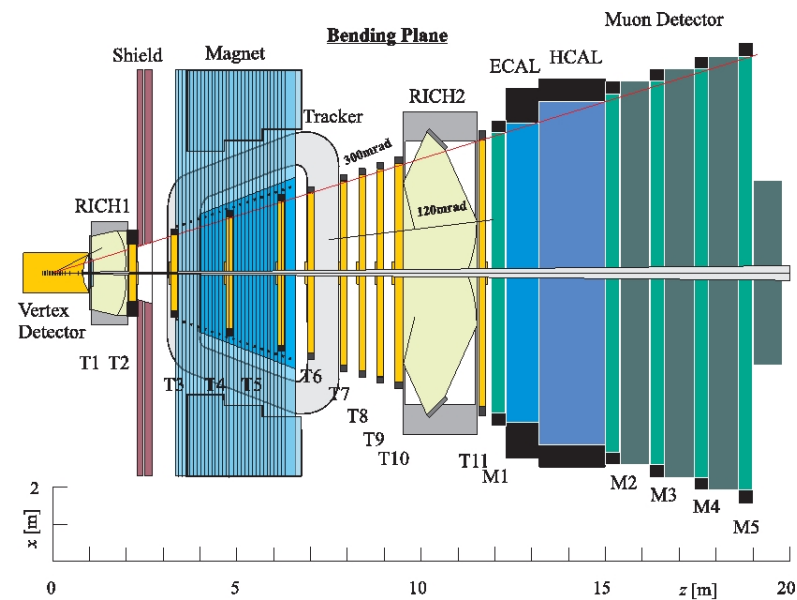


Figure 1.8: LHCb detector view from the top. ©CERN

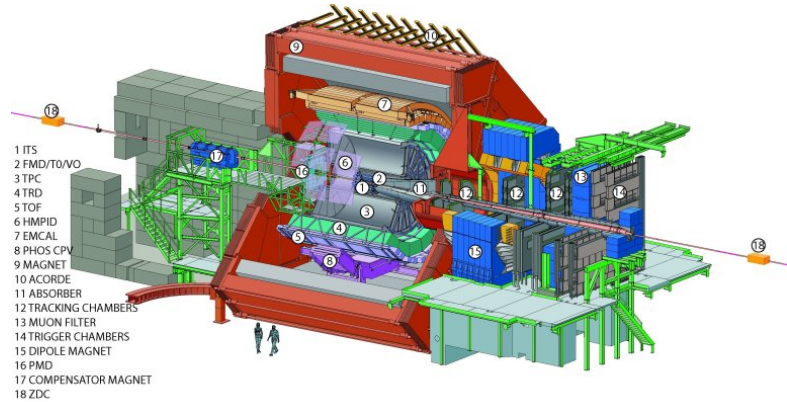


Figure 1.9: ALICE detector internal view. ©CERN

## 180 1.2 The Compact Muon Solenoid (CMS) experiment

181 The CMS detector, hosted at point 5 of the LHC main ring (see figure 1.2), is the second  
182 biggest LHC experiment. Cylindrically shaped, measures 15 m of diameter and 28.7 m  
183 long, and weights 14000, making it the heaviest LHC experiment. Its subsystems are  
184 concentrically located from the collision point in the beam line. Its main characteristic  
185 is the strong 3.8 T solenoid magnet. A representation of the detector can be found in  
186 figure 1.10. The CMS collaboration is formed by around 2600 scientists, of which 900  
187 are students, from 181 institutes over 41 countries.

188 CMS has been designed to be able to do very precise identification of particles origi-  
189 nated from the collisions and their properties. For the measurement of the momentum  
190 of the charged particles, CMS counts with a very strong magnet that allows to bend very  
191 energetic particles. In addition, the calorimeters allow to measure accurately the energy  
192 from hadrons, electrons and photons. At the most external layer, the muons chambers  
193 measuring muons properties, and in the innermost the tracking system that reconstructs  
194 the collision points and the charged particles tracks. In figure 1.11 can be found a repre-  
195 sentation of the different subsystems of CMS and how particles are reconstructed from  
196 them.

### 197 1.2.1 Coordinate system

198 The origin of coordinates defined on the CMS detector is located on the nominal collision  
199 point, the “interaction point”. From there, the z-axis is defined along the beam pipe line  
200 pointing towards the Jura mountains. The positive/negative z-axis directions define the  
201 positive/negative sides of the detector. The y-axis is defined towards the zenith and the  
202 x-axis towards the center of the LHC ring. Due to the inclination of the LHC plane, this  
203 coordinate system is slightly tilted with respect to the true vertical. A representation of  
204 the coordinate system definition can be found in figure 1.12.

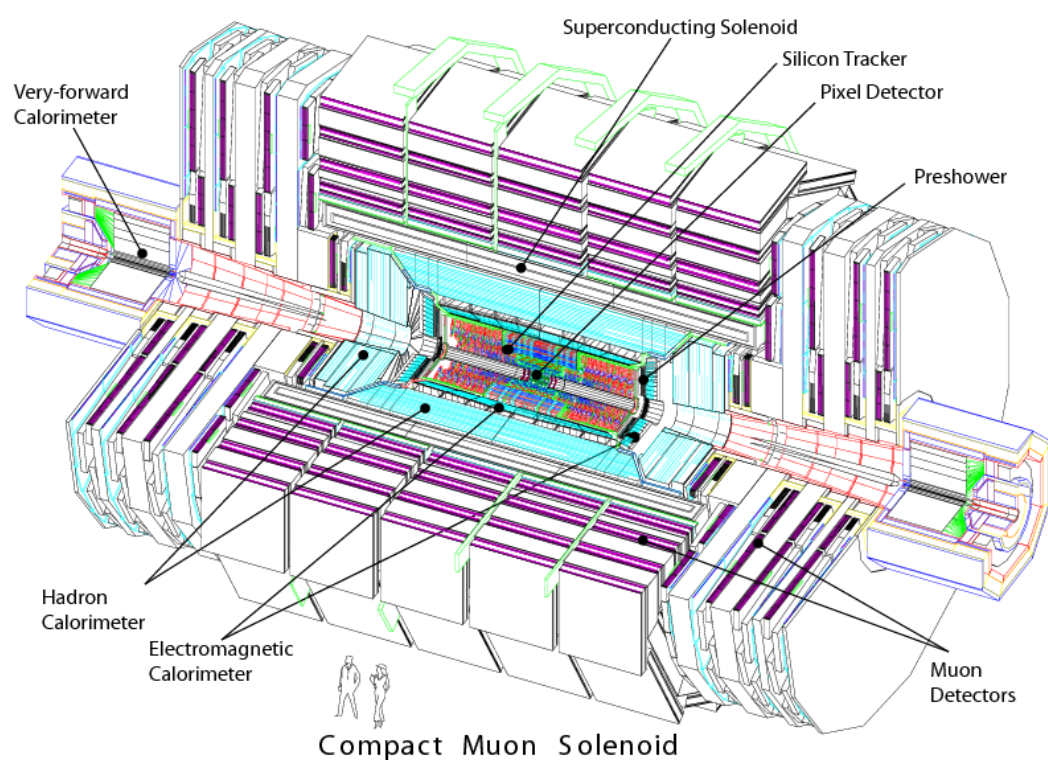


Figure 1.10: CMS detector internal view. ©CERN

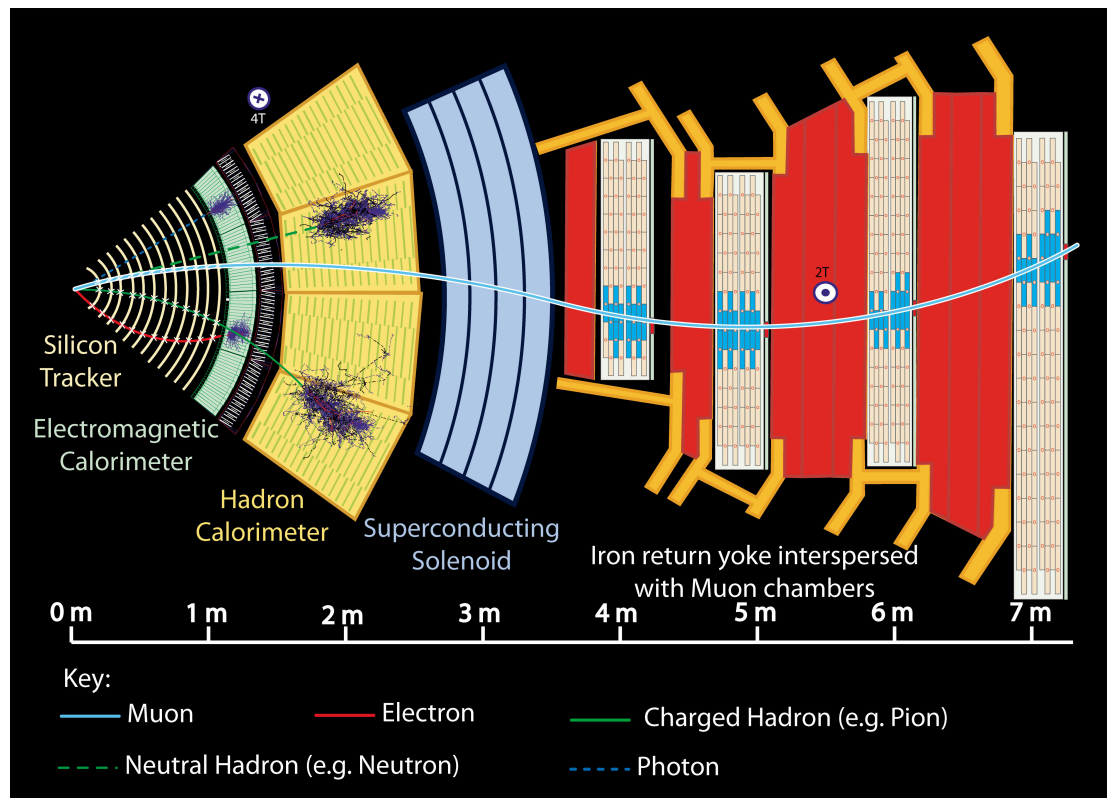


Figure 1.11: CMS sub-detectors and particle identification. ©CERN

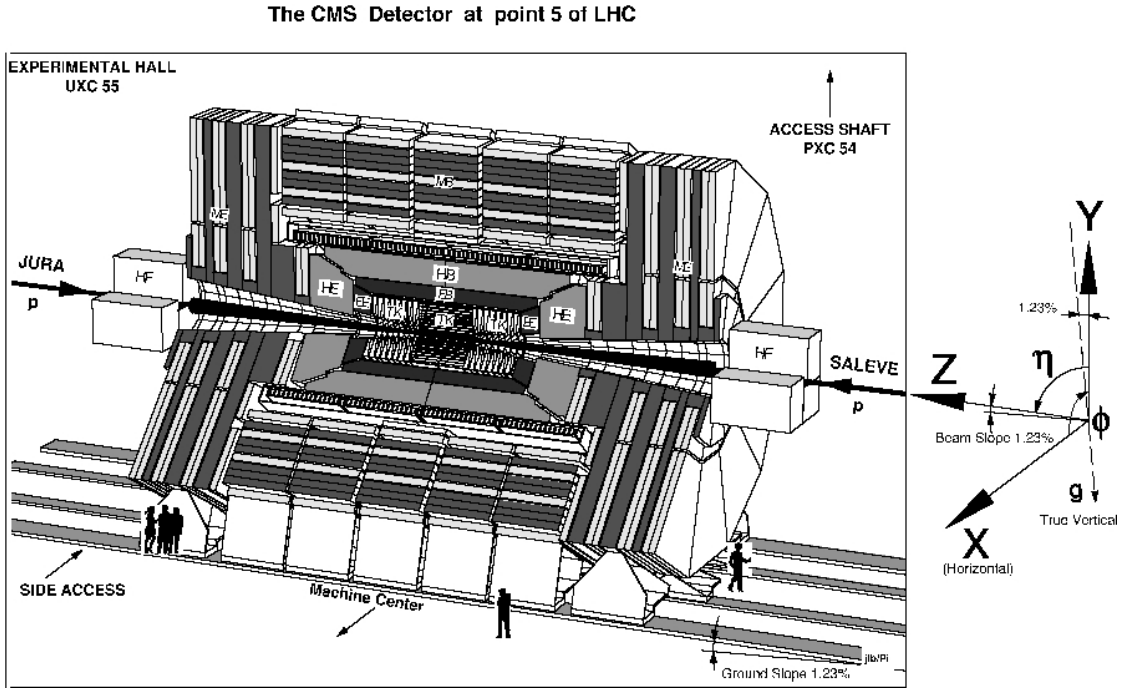


Figure 1.12: CMS coordinate system. ©CERN

205 We can also define two angles: the  $\phi$  angle in the x-y plane from the x-axis towards the  
 206 positive y-axis, and the  $\theta$  angle in the z-y plane from z-axis towards the positive y-axis.  
 207 In experimental particle physics is preferred to work with relativistic invariant quantities,  
 208 reason why instead of working with  $\theta$  we define the pseudorapidity  $\eta$ , equation 1.3.

$$\eta = -\ln \left( \tan \left( \frac{\theta}{2} \right) \right) \quad (1.3)$$

209 One can define another relativistic invariant quantity, the rapidity  $y$  as from equa-  
 210 tion 1.4. With  $\mathbf{p}$  being the momentum vector and  $E$  the energy of a given particle,  $p_L$   
 211 denotes its longitudinal component, that in our case is the same z-component.

$$y = \frac{1}{2} \ln \left( \frac{E + p_L}{E - p_L} \right) \quad (1.4)$$

212 On the limit that the mass of the particle is very small compared to its momentum,  
 213 one can replace approximate the particle energy by the momentum magnitude, giving  
 214 rise to the definition of the pseudorapidity in terms of the momentum of the particle  
 215  $\eta = \frac{1}{2} \ln \left( \frac{\mathbf{p} + p_L}{\mathbf{p} - p_L} \right)$

216 We define also the radial coordinate over the x-y plane, plane that is called the  
 217 transverse plane being orthogonal to the longitudinal direction, the z-axis. In such plane  
 218 are also defined the transverse quantities of particles, as the transverse momentum  $\mathbf{p}_T$ .

219 Finally, for any two objects an angular distance can be defined in the  $\eta - \phi$  plane, as in  
 220 equation 1.5.

$$\Delta R = \sqrt{(\Delta\eta)^2 + (\Delta\phi)^2} \quad (1.5)$$

221 **1.2.2 Magnet**

222 In order to measure the momentum of the charged particles going inside the detector  
 223 is crucial to apply the correct magnet field, sufficiently strong to bend very energetic  
 224 particles. The momentum of a charged particle inside an uniform magnetic field can be  
 225 written as

$$p = \gamma mv = qBr \quad (1.6)$$

226 where  $B$  is the magnitude of the magnetic field,  $\gamma$  the usual relativistic factor,  $m$  the  
 227 mass of the particle,  $v$  its rapidity,  $q$  its charge and  $r$  the bending radius. The sagitta of  
 228 the arc is

$$s = \frac{L^2}{8r} = \frac{qBL^2}{8p} \quad (1.7)$$

229 with  $L$  the distance the particle moved inside the magnetic filed. Inside a solenoid  $L$  is  
 230 equal to the radius of it.

231 From relation 1.7 is possible to deduce that the resolution on the momentum of the  
 232 particle has an inverse dependence with the magnetic field and the radius of the solenoid,  
 233 as shown in equation 1.8. From there, for a better resolution is needed to increase the  
 234 magnetic field and the radius of the solenoid.

$$\frac{dp}{p} \propto \frac{p}{BL^2} \quad (1.8)$$

235 The design of CMS magnet target both features, it utilizes a large solenoid of 6 m of  
 236 diameter and 13 m long. It's made of 4 layers of windings of NbTi cable that is cooled  
 237 to 4.45 K in order to achieve the superconducting state. This magnet is able to produce  
 238 an uniform magnetic field inside of it of 3.8 T. Outside the magnet 5 wheels and 3 disks  
 239 of iron are placed in order to return the flux of the magnetic field, inducing just a 2 T  
 240 radial magnetic field outside the solenoid. This iron yoke contributes with most of the  
 241 weight of the detector, 10000 tons. In between the iron yoke the muon chambers are  
 242 placed.

243 **1.2.3 Tracker system**

244 The tracker system has been designed to specifically address the reconstruction of high  
 245 pt leptons, with particular interest in the isolation of electrons and, as a consequence, to  
 246 isolate photons. Also the tracker fulfill granularity requirements to reconstruct secondary  
 247 vertexes to tag and reconstruct B-hadrons. The tracker system is able to reconstruct

248 tracks of particles with at least 2 GeV of  $p_T$  with  $|\eta| < 2.5$ . Charged hadrons are  
 249 reconstructed with an efficiency of at least 85% for  $p_T = 1$  GeV and up to 95% for  $p_T$   
 250 above 10 GeV. Another important point that was taken into account is the fact that the  
 251 tracker is the part of CMS most exposed to radiation as it is the closest subsystem to  
 252 the interaction point. The tracker system was built highly resistant to radiation damage  
 253 and is expected to last for around 10 years. The pixel detector only lasts 2 years and  
 254 was replaces during LS1.

255 The tracker has been built with three different technologies: Pixels, Silicon Strips and  
 256 Micro Strip Gas Chambers (MSGCs). They are arranged concentrically in cylindrical  
 257 volumes being the pixel detector the innermost and the MSGCs the outermost. The  
 258 CMS tracker extends to a radius of 155 cm and a around 270 cm on each  $z$  direction.  
 259 The pixel system is in the region with a radius below  $\approx 20$  cm, the silicon detector  
 260 between  $\approx 20$  cm and  $\approx 60$  cm, and the MSGCs between  $\approx 70$  cm and  $\approx 120$  cm. The  
 261 three subsystems are fast enough to work at 25 ns scale.

262 The pixel system is formed by three barrel layers and two end caps disks covering  
 263 radii from 6 cm to 15 cm. It has an approximate active surface of one square meter with  
 264 approximately  $40 \times 10^6$  channels with a cell size of 150  $\mu\text{m}$  by 150  $\mu\text{m}$ . This pixel system  
 265 allows to obtain three highly precise points that are mainly used for reconstructing  
 266 vertexes.

267 The Silicon Strip system is formed by a 5-layer barrel (TIB for Tracker Inner Barrel)  
 268 and 10 disks (TID for Tracker Inner Disks) in each end cap. The strips length is 12.5  
 269 cm with a pitch from 61  $\mu\text{m}$  to 122  $\mu\text{m}$  for single-sided strips and for 81  $\mu\text{m}$  to 244  $\mu\text{m}$   
 270 for double-sided. It's able to achieve a hit resolution of about 15  $\mu\text{m}$ .

271 The MSGCs systems is composed of 6 layers in the barrel (TOB for Tracker Outer  
 272 Barrel) and 11 disks in each end cap (TEC for Tracker EndCap, with a  $\pm$  sign depending  
 273 on the  $z$  direction). Here the strips are 10 cm length for the inner layers and 25 cm for  
 274 outer layers with a pitch from 200  $\mu\text{m}$  to 400  $\mu\text{m}$ , which gives a hit resolution of 35  $\mu\text{m}$   
 275 and 100  $\mu\text{m}$  respectively. The MSGCs and Silicon systems have an overall active area of  
 276 around 300  $\text{m}^2$  with  $12 \times 10^6$  channels organized in more than ten thousand independent  
 277 modules.

278 In figure 1.13 can be seen the disposition of all the tracker subsystems. From the  
 279 design of the tracker system the best resolution on the  $p_T$  measurement is achieved in  
 280 the  $|\eta| < 1.6$  region, this due to the presence of more layers of detector in the different  
 281 subsystems, as shown in figure 1.14.

#### 282 1.2.4 Electromagnetic calorimeter

283 The CMS ECAL (Electromagnetic CALorimeter) is the detector subsystem designed  
 284 to stop photons and electrons to measure their energy. It's an hermetic cylindrical  
 285 calorimeter made of 61200 crystals in the barrel ( $|\eta| < 1.479$ ) and 7324 in each end  
 286 cap ( $1.48 < |\eta| < 3$ ). The crystals material is lead-tungstate that is transparent, very  
 287 dense ( $8.28 \text{ g/cm}^3$ ), has a small Moliere radius (2.2 cm) and a short radiation depth  
 288 ( $X_0 = 0.89 \text{ cm}$ ). This material has been chosen for the characteristics already described,  
 289 but also because is very fast emitting the scintillation light (in 25 ns), it has a very good

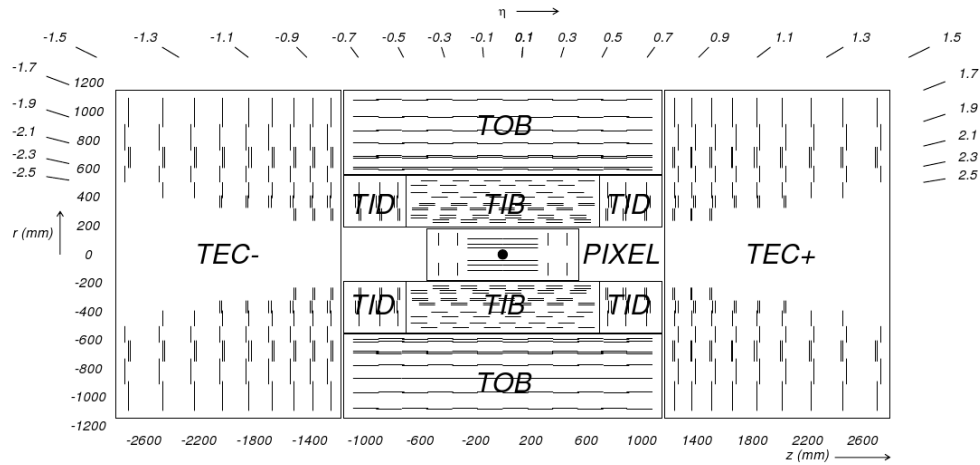
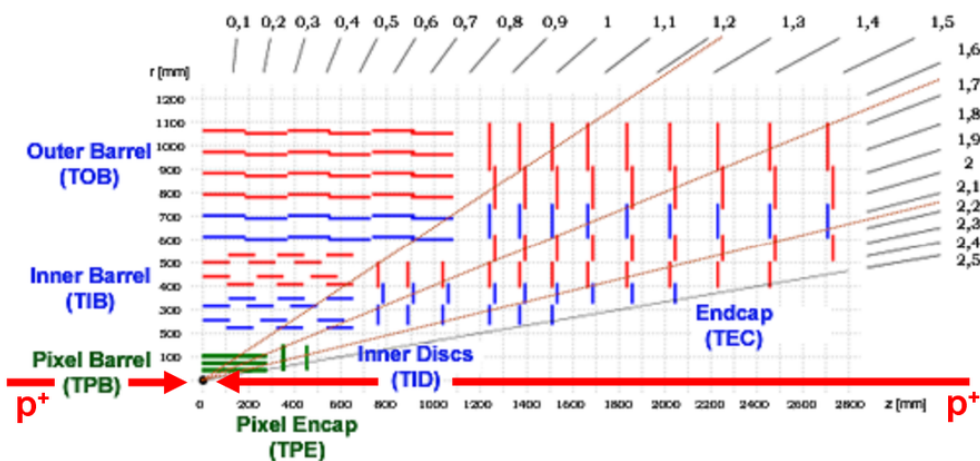


Figure 1.13: CMS tracker system configuration. ©CERN

Figure 1.14: Tracker resolution with  $\eta$ . ©CERN

290 energy resolution and resistance to radiation. The crystals are distributed in 36 super-  
 291 modules, 1700 crystals each, in the barrel (EB for ECAL Barrel) and in four 'Dee's, of  
 292 3662 crystals each, in the end caps (EE for ECAL End cap). In the EB the scintillation  
 293 light is collected by Avalanche Photo-Diodes, or APD, and by Vacuum Photo-Triodes,  
 294 or VPT, in the EE. A preshower system is installed in face of each end cap to allow a  
 295 better discrimination between photons and  $\pi^0$ 's. A representation of the CMS ECAL  
 296 can be found on figure 1.15.

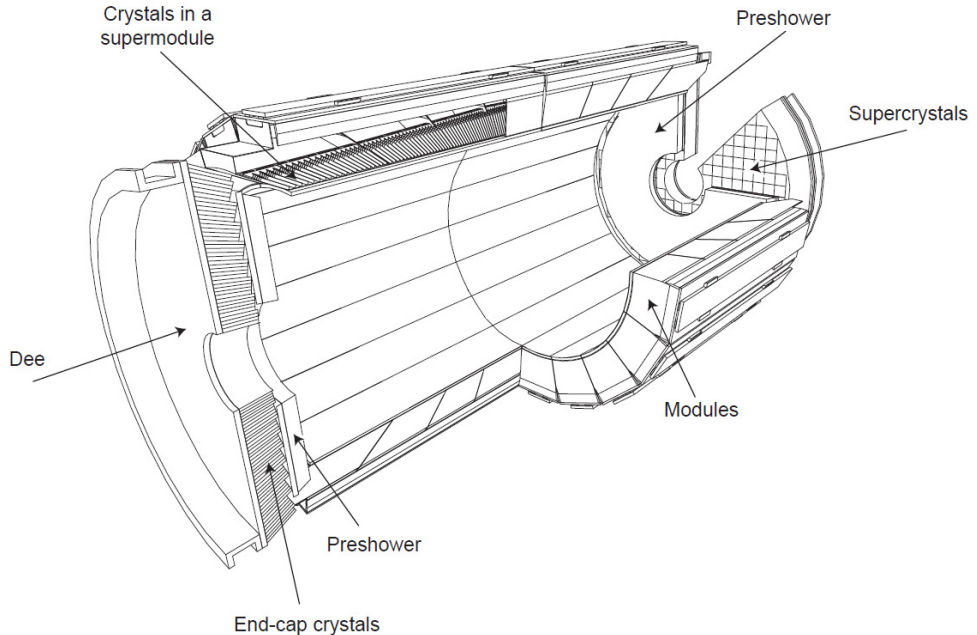


Figure 1.15: CMS ECAL representation. ©CERN

### 297 1.2.5 Hadronic Calorimeter

298 The CMS HCAL, for Hadronic CALorimeter, is the subdetector designed to measure  
 299 the energy of hadrons produced in the collisions, mainly the neutral hadrons because  
 300 the charged hadrons are already traced by the tracker. It's also designed to measure the  
 301 missing energy coming from particles not being detected by any of the subsystems, as  
 302 neutrinos. It's an hermetic set of subsystems covering up to  $|\eta| < 5.2$ :

- 303 • Hadron Barrel Calorimeter (HB): Covering  $|\eta| < 1.4$  is located between the ECAL  
 304 barrel and the magnet.
- 305 • Hadron Endcap Calorimeter (HE): Extends the coverage of the barrel on the region  
 306  $1.4 < |\eta| < 3$ .

- Hadron Outer Calorimeter (HO): Located outside the magnet, uses it as an additional absorber.
- Hadron Forward Calorimeter (HF): Completes the coverage of the system from  $|\eta| = 3$  up to  $|\eta| = 5.2$ .

The CMS HCAL layout is shown in figure 1.16. The system is made of two parts, an absorber to develop the hadronic showers and a scintillator to measure the particles energy. The length scale of hadronic calorimetry is designated as the interaction length corresponding to the mean free path of an hadron in a material. The HB absorber is made of 40 mm thick steel plate, eight layers of brass plates of 50.5 mm thick, six brass plates of 56.5 mm thick and a steel plate of 75 mm thick. The HE uses the same absorber but with thicker plates, of 79 mm. Between the absorber plates a plastic scintillator, Kuraray SCSN81, of 3.7 mm thick is placed. In the region with  $|\eta| < 1.6$  the achieved granularity is  $\Delta\eta \times \Delta\phi = 0.087 \times 0.087$  and  $\Delta\eta \times \Delta\phi = 0.17 \times 0.17$  in the region with  $|\eta| > 1.6$ . This design gives a total of 70000 tiles used. The produced light in the HB is collected by optical fibers and transferred to the Hybrid Photo Diodes (HPDs). This diodes were chosen thanks to their small sensitivity to the magnetic field, an important feature due to the proximity of the HCAL to the magnet.

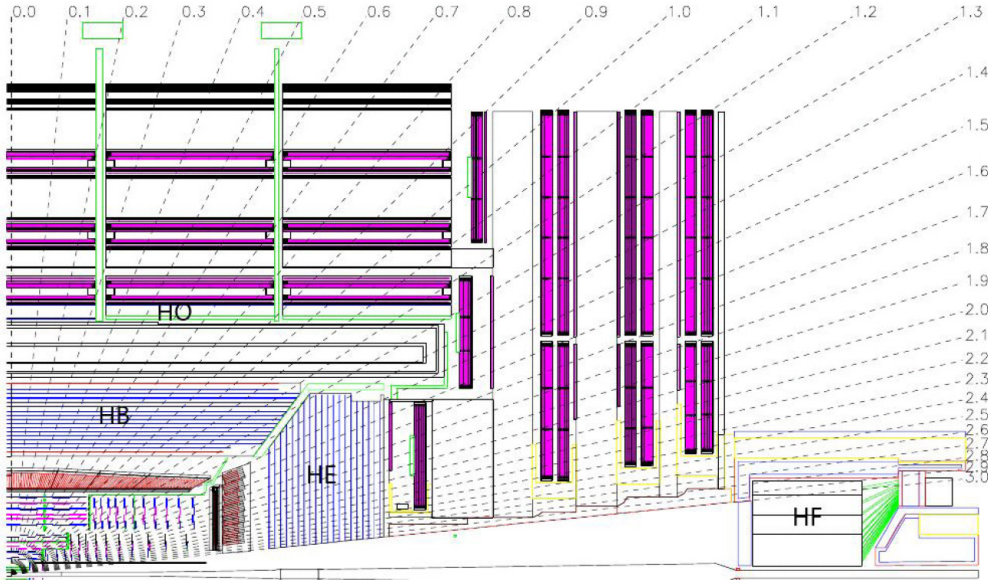


Figure 1.16: CMS HCAL representation. ©CERN

The HF design is very different from the rest of the HCAL subsystems. The most important challenge for the HF is the high resistance to radiation, while in the central rapidity region 100 GeV are deposited in average in the forward region is 760 GeV. For this reason it was chosen a Cherenkov detector made of quartz fibers with a steel absorber. The light produced in the HF is collected by photo multipliers.

329 **1.2.6 Muon chambers**

330 The muon system of CMS is located at the most exterior layer of the detector due to  
331 the penetration power of this particle. Muons are not stopped by the calorimeters and,  
332 with neutrinos, they are able to escape the detector. The muon chambers are placed in  
333 a cylinder around the HO and in disks on the end caps. Three main characteristics have  
334 been fulfilled from the design: efficient muon identification, precision measurement of  
335 muon charge and momentum and fast measurement to provide trigger capabilities. The  
336 moun chambers are made of three different subsystems:

- 337 • Drift Tubes Chambers (DT): Located in the region with  $|\eta| < 1.2$  and disposed in  
338 four layers. They consist of individual drift tubes of  $50 \mu\text{m}$  of diameter anode wire  
339 with two electrode plates creating a drift electric field. The wall of the cell act as  
340 cathode. The cells are filled with a gas mixture, 85% Argon and 15%  $\text{CO}_2$ . The  
341 tubes are organized in plaques that are also organized in SuperLayers (SL) each  
342 one made of 4 plaques. The barrel is made of 250 DT's disposed in four cylinders  
343 separated by iron yokes.
- 344 • Cathode Strip Chambers (CSC): Installed in the end caps, provide a coverage up  
345 to  $|\eta| = 2.4$  from  $|\eta| = 0.9$ . These chambers are multi-wire proportional chambers  
346 made of six planes of anode wires with 7 cathode planes. Four CSC stations  
347 are placed in each end cap. The wires are oriented in azimuthal direction while  
348 the cathode planes are radially oriented, allowing a complete measurement of the  
349 position of the particle. This system is able to measure with a precision between  
350 the  $75 \mu\text{m}$  and  $150 \mu\text{m}$ .
- 351 • Resistive Plate Chambers (RPC): This subsystem is made of gaseous parallel plate  
352 detectors. This detector is specially useful for triggering as it is very fast and have  
353 a good position resolution. There are 480 RPC distributed in 6 layers in the barrel  
354 with the DT and in 3 layers in the end caps with the CSC, and covers the region  
355 with  $|\eta| < 1.6$ .

356 On figure 1.17 can be found a representation of the muon system with the different  
357 components. The DT and CSC system cover  $|\eta| < 2.4$  without any gap.

358 **1.2.7 Trigger**

359 LHC has been designed to provide experiments with proton-proton collisions every 25  
360 ns, meaning a frequency of 40 MHz. Each recorded event by CMS has a nominal size  
361 between 0.5 and 1 MB, what means a data flux of around  $10^9 \text{ MB/s} = 1\text{PB/s}$  that is  
362 extremely big for transfer and for storing. Therefore, an on-line selection of events has  
363 to be done. The trigger system of CMS does this task in two fold, a level 1 (L1) and a  
364 high level trigger (HLT). The L1 is hardware based and the HLT is software based.

365 From the searches conducted at CMS, the interesting events produced on proton-  
366 proton collisions for new physics searches are very rare. The enormous majority of  
367 events coming from proton-proton collisions correspond to well understood phenomena,

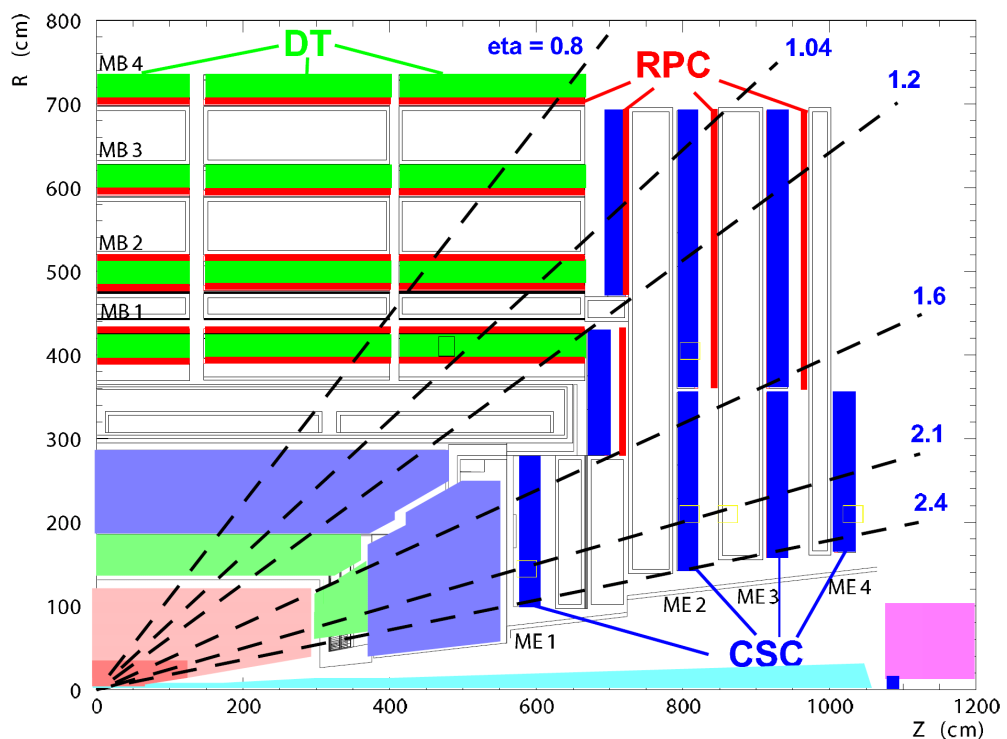


Figure 1.17: CMS muon chambers representation. ©CERN

368 while new physics events are ‘exotic’ with regards to the most common type of events.  
 369 Then is interesting to keep only a part of the events, what actually easies the analysis  
 370 afterward done over the data.

371 The CMS trigger system is designed to keep only 100 kHz tops by the L1 and 300 Hz  
 372 by the HLT. L1 is reducing the data flux by 2 orders of magnitude and the HLT another  
 373 3 orders of magnitude.

### 374 **Level 1 trigger**

375 The L1 is designed to trigger over coarse data coming from the calorimeters and muon  
 376 chambers, holding data in pipe-lined memories in the front-end electronics. There-  
 377 fore, relies on very fast reconstruction of objects coming from this subsystems: muons,  
 378 electrons, photons, jets and missing energy. This reconstruction differs from the final  
 379 reconstruction of the objects, for example a jet for the L1 consists on successive energy  
 380 deposits in the ECAL and HCAL, while the off-line reconstruction take into account  
 381 also the tracker information.

382 The L1 starts from regional data coming from the subsystems which is afterward  
 383 combined in order to build ranked trigger objects in localized regions of the detector.  
 384 Global Muon and Calorimeter triggers sort the objects and send the best ranked to the  
 385 Global Trigger (GT). Before the GT no events are rejected, is only with the GT that  
 386 the selection is applied. The GT combines the information and can apply topological  
 387 requirements and take a decision on keeping or disregarding the event. On figure 1.18  
 388 can be found the work-flow of the L1.

389 The L1 cards are distributed between the detector and an adjoin cavern at 90 m  
 390 distance from the detector. The latency time L1 disposes between the collision and the  
 391 taking of the decision is about  $3.2 \mu\text{s}$ . Therefore, the front-end memory in the cards  
 392 should be able to keep in memory up to 128 bunch crossings.

### 393 **High Level Trigger**

394 The HLT take as input the events accepted by the L1 and process them using farms  
 395 of commercial processors. The HLT does additional operations on the selected events  
 396 making it much slower than L1 processing. In particular, the HLT takes also into account  
 397 the tracker information. Consequently, this system is able to take into consideration the  
 398 whole information of the detector. However, the reconstruction of objects done by the  
 399 HLT differs slightly from the final off-line reconstruction. The decision taking process  
 400 takes around 40 ms,  $10^4$  times more than for L1.

401 The events selected by HLT are finally stocked on disks under several paths depending  
 402 on the selection performed. There is a constant development of HLT paths focusing on  
 403 different analysis requirements in order to obtain the best possible selection efficiency  
 404 for specific signal types.

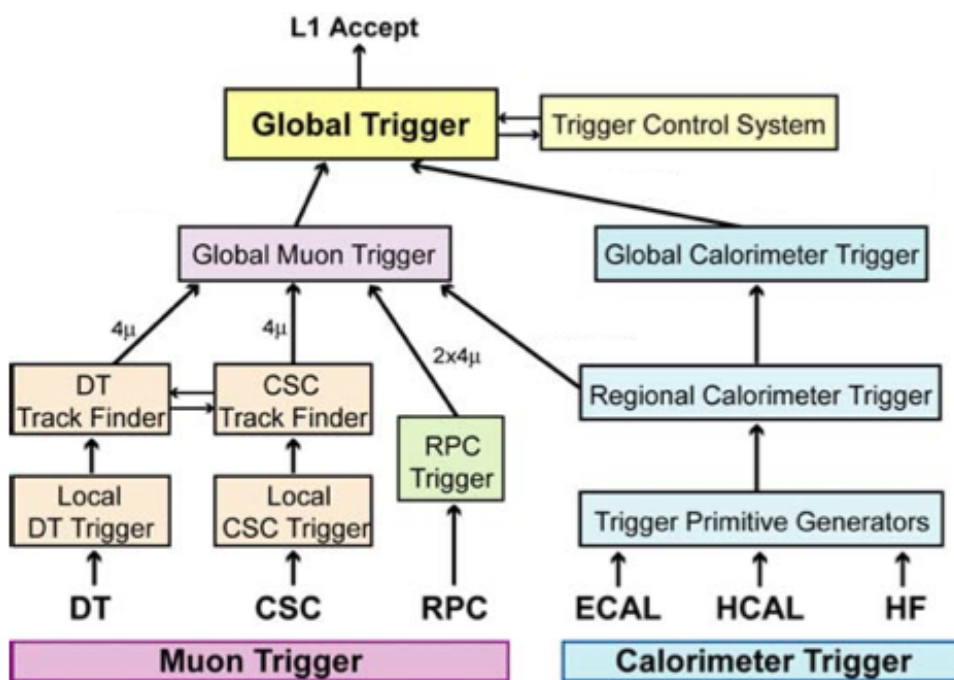


Figure 1.18: L1 architecture. ©CERN



405 **Chapter 2**

406 **The Standard Model**

407 Since the Greeks, different theories about the composition and structure of the world have  
408 been formulated. At ancient Greece these theories were elaborated from a philosophical  
409 point of view. Nowadays, we count with a very sophisticated set of tools and concepts  
410 that allowed us to build up a general vision of nature, its components and structure.  
411 Moreover, on the subject of the constituents, or elemental constituents, a theory capable  
412 of describing the majority of known phenomena has been developed. This theory is the  
413 Standard Model (SM) of particle physics.

414 This SM relies in two of the more elegant constructs of modern physics and math-  
415 ematics. From the physics side, the quantum field theory; from mathematics, group  
416 theory. Quantum field theory has born from the understanding of processes that take  
417 place at very small spatial scales and in a regime where special relativity play an im-  
418 portant role. To describe such, a major part of the most brilliant minds of the 20th  
419 century dedicated their life, Paul Dirac, Richard Feynman, Enrico Fermi among them.  
420 The theory of quantum fields has set in a common place two extraordinary achievements  
421 of physics: special relativity and quantum mechanics. With it we have been capable to  
422 describe many phenomena:  $\beta$  and  $\alpha$  decay, solid state, among many other.

423 From the mathematics side, group theory has become one of the most powerful tools  
424 for particle physicist. However, their development began quite early, with Galois around  
425 1830, and was used in other parts of physics, it's with Lie algebras and the possibility of  
426 describing continuous symmetries that the most important step were given. Also, this  
427 would have not been possible with the amazing connection found by Emmy Noether in  
428 1918. She found that for every conserved quantity there is a preserved symmetry. Group  
429 theory can be seen, roughly speaking, a way to mathematically describe symmetries,  
430 group theory became the tool to describe systems with conserved quantities.

431 In this chapter, we present the basics of the SM. We describe its seminal ideas, its  
432 structure and content and its ultimate consequences. Finally, we close with its limita-  
433 tions.

## 434 2.1 Fields, symmetries and interactions

435 From the very beginning of physics, one of the most fundamental questions has been how  
 436 does bodies interact, and what is exactly an interaction. On the first type of interaction  
 437 ever studied by physics, gravity, Newton proposed the concept of distant interaction,  
 438 the idea that bodies could interact without being in direct contact. But the question on  
 439 how exactly that distant action was performed remained unanswered.

440 During the 19th and 20th century new phenomena were discovered pointing to brand  
 441 new interactions, electricity, magnetism and radioactivity. The very precise and com-  
 442 plete description of electromagnetism developed by Gauss, Faraday, Ampère and finished  
 443 by Maxwell arrived to describe electricity and magnetism under the formalism of only  
 444 one interaction within the mathematical formalism of classical fields. Further works  
 445 addressed radioactivity, driving to a deeper understanding of nature and its composition.

446 For the following discussion, and later, we are going to work in natural units for  
 447 simplicity. In these units the speed of light  $c$  is normalized to unity, as well as electron  
 448 electric charge  $e$ , reduced Planck constant  $\hbar$  and Boltzmann constant  $k_B$ . Then, masses  
 449 and temperature are expressed in energy units, i.e.  $eV$ , and time and length in inverse  
 450 energy units,  $eV^{-1}$ .

451 A classical field is an assignment of a quantity to every point in space and time. For  
 452 physics, the quantity that is attributed it's a physical quantity such as mass, electrical  
 453 charge or probability. This quantity can be scalar or vector, giving rise to the notion  
 454 of scalar or vector field, correspondingly. As an example, a fluid can be described in  
 455 terms of fields, being the velocity of the fluid a vector field and its pressure a scalar field.  
 456 Generic classical electromagnetic interactions can be described with the help of one  
 457 vector field  $\vec{A}(x)$ , the vector potential, and one scalar field  $\phi(x)$ , the scalar potential.  
 458 In the formalism of four-vectors from relativistic dynamics one can organize these two  
 459 quantities in the four-potential  $A_\mu = (-\phi, \vec{A})$ . This can be used to define the strength  
 460 field tensor  $F_{\mu\nu} = \partial_\mu A_\nu - \partial_\nu A_\mu$ , where  $\partial_\mu = \left(-\frac{\partial}{\partial t}, \nabla\right)$  is the covariant derivative. From  
 461 the tensor it is possible to obtain in a very generic and elegant way the equations of motion  
 462 of the free field using the Lagrangian formalism, as in equation 2.1. With the Lagrangian  
 463 density defined in equation 2.2.

$$\partial_\mu \left( \frac{\partial \mathcal{L}}{\partial(\partial_\mu A_\nu)} \right) - \frac{\partial \mathcal{L}}{\partial A_\nu} = 0 \quad (2.1)$$

$$\mathcal{L} = -\frac{1}{4} F^{\mu\nu} F_{\mu\nu} \quad (2.2)$$

464 It's very important to notice that the equations of motion of the free field are invariant  
 465 under the choice of the four-potential. More precisely, the covariant potential is not  
 466 unique and we can always add the covariant derivative of a scalar field,

$$A'_\mu = A_\mu + \partial_\mu \Lambda(x) \leftrightarrow \partial^\mu A_\mu = 0 \quad (2.3)$$

467 and describe the same physics. This non-uniqueness corresponds to the choice of a zero-  
 468 point of the potential very well known in non-Lagrangian formalism of electrodynamics.

469 When we choose a specific value for this scalar field,  $\Lambda(x)$ , we say that the gauge has  
 470 been fixed.

471 One can also define a four current vector,  $J_\mu = (\rho, \vec{J})$  with  $\rho$  the electric charge  
 472 density and  $\vec{J}$  the current charge density. Then, plugging in the four current in the  
 473 Lagrangian of the free field, defined in equation 2.2,

$$\mathcal{L} = -\frac{1}{4}F^{\mu\nu}F_{\mu\nu} - A_\mu J^\mu \quad (2.4)$$

474 we can obtain the complete set of equations of motion of the field with charges and  
 475 currents.

476 The transformation stated from equation 2.3 can be understood as a transformation  
 477 of the field. These type of transformations are mathematically understood under the  
 478 group  $U(1)$ , where the generic transformation operator can be written as  $U = e^{i\theta(x)}$ .  
 479 It's said then that the electromagnetic vector potential is *invariant* under  $U(1)$   
 480 transformations. This property identifies an essential characteristic of electromagnetism, its  
 481 symmetric behavior under  $U(1)$ .

482 From this reasoning the most interesting results are drawn when the same symmetry  
 483 is imposed to another fields. For example, the kinetic Lagrangian for a complex scalar  
 484 field is  $\mathcal{L} = (\partial^\mu\phi)^*\partial_\mu\phi$ . To perform the transformation over the scalar field is sufficient to  
 485 apply the operator as  $\phi' = U\phi$  and  $\phi'^* = \phi^*U^{-1}$ . But it's evident that the Lagrangian  
 486 is not the same after applying such transformation. Then, in order to preserve the  
 487 Lagrangian under  $U(1)$  is necessary to change at the same time the derivative. Such  
 488 transformation is given in equation 2.5, where  $g$  is a constant.

$$\mathcal{D}^\mu = \partial^\mu - igA^\mu \quad (2.5)$$

489 Then, the proposed Lagrangian can be rewritten, including the vector field, as

$$\mathcal{L} = (\mathcal{D}^\mu\phi)^*\mathcal{D}_\mu\phi - \frac{1}{4}F^{\mu\nu}F_{\mu\nu} \quad (2.6)$$

490 that is invariant under  $U(1)$ . From the kinematic term with the new derivative inter-  
 491 action terms between the scalar and the vector field can be derived, as  $igA^\mu\phi^*\partial_\mu$ . This  
 492 shows that the requirement of the invariance under  $U(1)$  of the scalar field lead to the  
 493 introduction of an interaction with a vector field controlled by the constant  $g$ . We have  
 494 also seen that electromagnetic interaction is described precisely by a vector field and  
 495 that preserves  $U(1)$  symmetry. What implies that this symmetry is the connection to  
 496 electromagnetic interaction, identifying the interaction itself with the  $U(1)$  symmetry.  
 497 In addition, using Noether theorem one can show that  $g$  is a conserved quantity, as the  
 498 electric charge is.

499 But not only electromagnetism can be described via a continuous symmetry as  $U(1)$ .  
 500 On 1896 radioactivity was discovered by the french physicist Henri Becquerel. Three  
 501 years after, Marie and Pierre Curie studied in more detail the phenomenon and found  
 502 Polonium and Radium elements. And later on, Ernst Rutherford was able to describe  
 503 radioactivity as coming in three types, alpha ( $\alpha$ ), beta ( $\beta$ ) and gamma ( $\gamma$ ). He also

504 noticed that radioactivity was able to change matter, which allowed him, with also  
 505 other experiences, to propose an atomic model, describing elements as basically and  
 506 external core of negative charges and a nucleus positively charged. Consequently, This  
 507 findings implied the existence of interactions different to electromagnetism, acting at the  
 508 atomic scale.

509 The interaction that undergoes radioactivity, beta decay, is called the weak interaction.  
 510 In 1933 Enrico Fermi made a first theoretical description of this interaction, but  
 511 only in 1968 Sheldon Glashow, Abdus Salam and Steven Weinberg were able to describe  
 512 weak interaction with a symmetry group:  $SU(2)$ . Finally, the interaction that keeps the  
 513 nucleus components together, the strong interaction, was described with  $SU(3)$  group  
 514 mainly by Murray Gell-Mann in 1963.

515 There have been many attempts to describe gravity with the same formalism, but  
 516 up to present such attempts have been unsuccessful. Such question remains one of the  
 517 most important problems for modern particle physics.

## 518 2.2 Quantum fields and particles

519 Classical fields, introduced and described in last section 2.1, can be extended to a quan-  
 520 tum theory. Such procedure is known as the quantization of fields and allow to unify  
 521 special relativity and quantum mechanics in one theory, Quantum Field Theory (QFT),  
 522 to describe the dynamics of systems in such regimes: speed close to the speed of light  
 523 on the atomic or smaller scales.

524 Quantum mechanics introduced two fundamental concepts: first, the description  
 525 of the system by its states; and second, the identification of an observable with an  
 526 operator. The state of a system is identified with a set of quantum numbers that tell  
 527 us the characteristics of the system when is at some state. For example, the hydrogen  
 528 atom system has energy as quantum number, such that each state has a value for the  
 529 energy describing the potential energy contained in the system. Quantum states are  
 530 mathematically noted in Dirac notation as a *ket*,

$$|\alpha\rangle = |i, j, k, \dots\rangle \quad (2.7)$$

531 with  $\alpha$  the set of quantum numbers  $i, j, k, \dots$  This mathematical object lives in Hilbert  
 532 space (a complex space  $\mathbb{C}$  of functions), which conjugate, a *bra*, is noted  $\langle\alpha|$ , and their  
 533 internal product  $\langle\beta|\alpha\rangle$ . The numerical value of  $|\langle\beta|\alpha\rangle|^2$  gives the transition probability  
 534 of the system from state  $\beta$  to state  $\alpha$ , and  $|\langle\alpha|\alpha\rangle|^2$  is the probability to find the system  
 535 in state the  $\alpha$ .

536 Physical observables as position, energy or momentum are described by complex  
 537 operators such that to measure their value for a given state, one just have to calculate  
 538  $|\langle\alpha|\hat{O}|\alpha\rangle|^2$ . The identification of observables and operators is called *first quantization*.  
 539 In addition, Schrodinger equation describes the evolution of states,

$$\hat{\mathcal{H}}|\alpha\rangle = i\frac{d}{dt}|\alpha\rangle \quad (2.8)$$

540 with  $\mathcal{H}$  the Hamiltonian of the system. The whole formalism is able to explain *quantized*  
 541 systems, where the quantum numbers are discrete, such as hydrogen atom or black body.

542 Several functions or fields can be related to a given state. These functions, wave  
 543 functions, can be used as the states to calculate probabilities. In *second quantization*  
 544 wave functions are upgraded into field operators. This procedure gives rise to the quan-  
 545 tization of the state of the field, which is described by the quantum number  $n$  which is  
 546 definite positive.  $n = 0$  for the fundamental state and  $n > 0$  for the excited states. Such  
 547 excitations of the field are understood as physical particles that propagates in space-time,  
 548 which means that  $n = 0$  is vacuum.

549 The first QFT ever created was born from the quantization of the electromagnetic  
 550 field. Quantum Electro Dynamics (QED) is the quantized version of classical electrody-  
 551 namics, that was developed by Tomonaga, Schwinger and Feynman around 1960. This  
 552 theory describes electromagnetic interactions of a charged field and the electromagnetic  
 553 vector field. The charged field excitations correspond to electrons and the excitations  
 554 of the vector fields are photons, responsible of light. Electrons are a particle with nega-  
 555 tive electric charge and orbit around the nucleus in atoms. Discovered in 1897 by J. J.  
 556 Thomson, it was fully described by P. A. Dirac in 1928 with the Dirac equation that is  
 557 the Schrodinger equation for a relativistic particle of spin 1/2. Spin, the intrinsic angu-  
 558 lar momentum carried by a particle, can be integer (0,1,2,...) or semi-integer ( $\frac{1}{2}, \frac{3}{2}, \dots$ ).  
 559 The particles with semi-integer spin, as electrons, are called *fermions* and particles with  
 560 integer spin, as photons, are called *bosons*. Dirac equation predicted the existence of a  
 561 particle identical to the electron but with positive charge, the positron. It was discovered  
 562 on 1932 by Carl David Anderson.

563 Up to present days we have found 12 fundamental fermions and 5 fundamental  
 564 bosons. Fermions are organized in *leptons*, that don't interact strongly, and *quarks*,  
 565 that do interact strongly. Leptons are as well organized in three families, the electron  
 566 ( $e^-$ ) and electron neutrino ( $\nu_e$ ), muon ( $\mu^-$ ) and muon neutrino ( $\nu_\mu$ ) and tau ( $\tau$ ) and  
 567 tau neutrino ( $\nu_\tau$ ). Electron, muon and tau are electrically charged while neutrinos are  
 568 neutral. Their respective anti-particles are equally organized, positron ( $e^+$ ) with elec-  
 569 tron anti-neutrino ( $\bar{\nu}_e$ ), anti-muon ( $\mu^+$ ) with muon anti-neutrino ( $\bar{\nu}_\mu$ ) and anti-tau ( $\tau^+$ )  
 570 with tau anti-neutrino ( $\bar{\nu}_\tau$ ). Quarks also come in three families, with the respective anti-  
 571 quarks: up ( $u, \bar{u}$ ) and down ( $d, \bar{d}$ ), charm ( $c, \bar{c}$ ) and strange ( $s, \bar{s}$ ), top ( $t, \bar{t}$ ) and bottom  
 572 ( $b, \bar{b}$ ). The fundamental bosons are the photon ( $A$ ), the W (positively and negatively  
 573 charged) and Z that mediate the electroweak interaction, the gluon ( $g$ ) mediating the  
 574 strong interaction and the Higgs ( $H$ ). The weak bosons were discovered at CERN in  
 575 1983 at the UA1 and UA2 collaborations over the SPS accelerator (described on sec-  
 576 tion 1.1.1). The Higgs boson has been discovered recently on 2012 by ATLAS and CMS  
 577 experiments at the LHC. The 2013 physics Nobel prize was awarded to Francois Englert  
 578 and Peter W. Higgs "for the theoretical discovery of a mechanism that contributes to  
 579 our understanding of the origin of mass of subatomic particles, and which recently was  
 580 confirmed through the discovery of the predicted fundamental particle, by the ATLAS  
 581 and CMS experiments at CERN's Large Hadron Collider".

<sup>582</sup> **2.2.1 The mass problem**

<sup>583</sup> Using the concepts developed on later sections about QFT and symmetries it's possible to  
<sup>584</sup> construct a whole theory giving rise to a precise description of particles and interactions  
<sup>585</sup> between them. But such a theory does not allow to have massive bosons, whereas masses  
<sup>586</sup> for fermions are allowed. A mass term for a fermion  $\psi$  is of the form

$$m_\psi \bar{\psi} \psi$$

<sup>587</sup> where  $m_\psi$  is the mass of the field.

<sup>588</sup> Under  $U(1)$  transformations,  $\psi' = U\psi$ , the mass term remains the same, what means  
<sup>589</sup> that is invariant under  $U(1)$  transformations. The same is not true for a boson. A mass  
<sup>590</sup> term for a boson  $A$ , can be written as

$$m_A A^\mu A_\mu \quad (2.9)$$

<sup>591</sup> where  $m_A$  is its mass.

<sup>592</sup> The  $U(1)$  transformation for the boson is  $A'^\mu = A^\mu + \delta^\mu \theta(x)$ . Applying such trans-  
<sup>593</sup> formation on the mass term 2.10 one can obtain the transformed term

$$m_A (A^\mu A_\mu + A^\mu \delta_\mu \theta(x) + \delta^\mu \theta(x) A_\mu + \delta^\mu \theta(x) \delta_\mu \theta(x)) \quad (2.10)$$

<sup>594</sup> where the last three terms make this term not invariant under  $U(1)$  transformations.  
<sup>595</sup> Consequently, one can say that a mass term for the boson destroy the invariance of the  
<sup>596</sup> theory under  $U(1)$  symmetry.

<sup>597</sup> Nonetheless there is no need for a theory of a massive photon, there is a need to  
<sup>598</sup> have massive bosons for weak interactions. There is a relation between the mass of  
<sup>599</sup> a boson and the range of the interaction mediated by it. Massless bosons transmit  
<sup>600</sup> long range interactions, as electromagnetism, but short range interactions, as the weak  
<sup>601</sup> interaction, are mediated by massive bosons. More precisely the interaction range is  
<sup>602</sup> inversely proportional to the mass of the boson, higher the mass shortest the range.  
<sup>603</sup> Such relation can be seen from the structure of the propagator, which is a mathematical  
<sup>604</sup> entity that describes the probability a particle has to travel a distance in a given time.  
<sup>605</sup> Such propagator, for a vector boson, has a generic form given in equation 2.11, where  
<sup>606</sup>  $k_\mu$  is the momentum carried by the boson. It's clear from this structure that a massive  
<sup>607</sup> boson has less probability to travel a long distance than a massless boson in a given  
<sup>608</sup> time.

$$\frac{g_{\mu\nu}}{k^2 - m^2 + i\epsilon} \quad (2.11)$$

<sup>609</sup> Then, as massive bosons are requires for weak interaction, somehow the  $SU(2)$  sym-  
<sup>610</sup> metry has to be broken. There are basically two ways to broke a symmetry:

- <sup>611</sup> • Explicit symmetry breaking: By the introduction of a symmetry breaking term in  
<sup>612</sup> the Lagrangian, as a mass term for the bosons.

- 613     • Spontaneous symmetry breaking: When the ground state of one field fail to be  
 614       invariant under the symmetry.

615     Explicit symmetry breaking is not an option, because the symmetry needs to be  
 616       preserved in the Lagrangian in order to introduce the interaction.

### 617   2.2.2 Spontaneous Symmetry Breaking

618     Several physical systems exhibit an spontaneous symmetry breaking. For example, a  
 619       pencil balanced on its tip is perfectly symmetric system around the vertical axis, however,  
 620       because of the instability of the system the pencil will eventually fall over. The final state  
 621       is stable but not symmetrical. This transition also decreased the potential energy of the  
 622       system, driving the system to its ground state. This means that whereas the system  
 623       had a symmetry the ground state does not show the symmetry. In general, symmetry  
 624       breaking is linked to phase transitions, as liquid to gas transition or magnetization of  
 625       a ferromagnet, covering a plethora of physical processes. To a greater extent, in recent  
 626       studies, [8], the emergence of life has been understood as a phase transition of matter.

627     To achieve an spontaneous symmetry breaking of  $SU(2)$  in QFT one should choose a  
 628       field for which its ground state, vacuum, will fail the symmetry. This means, in practical  
 629       terms, that such field will have a non-zero value in vacuum, leading to a presence of  
 630       particles coming from the field on theory vacua. If a fermion field is chosen, the vacuum  
 631       will show a preference on directionality depending on its spin orientation, what breaks  
 632       Poincaré symmetry imposed by special relativity. The same is true if a spin-1 bosonic  
 633       field is chosen for the task. In order to avoid this problem a spin-0 field should be used.  
 634     In addition, this field should be electrically neutral to avoid having a charged vacuum.

635     With all this properties in mind, taking a scalar doublet of  $SU(2)$ , defined on equa-  
 636       tion 2.12 where  $\phi^0$  and  $\phi^+$  are complex fields, the most general potential can be written  
 637       from two auto-interaction terms, in equation 2.13.

$$\Phi = \begin{pmatrix} \phi^+ \\ \phi^0 \end{pmatrix} = \begin{pmatrix} \phi^+ \\ \phi_{RE} - i\phi_{IM} \end{pmatrix} \quad (2.12)$$

$$V(\Phi) = \mu^2 \Phi^\dagger \Phi + \lambda (\Phi^\dagger \Phi)^2 \quad (2.13)$$

638     Such potential has a unique minimum for  $\lambda > 0$  and  $\mu^2 > 0$ , but for  $\lambda > 0$  and  
 639        $\mu^2 < 0$  has a set of minima with the shape of “Mexican hat”, shown in figure 2.1. Under  
 640        $\lambda > 0$ ,  $\mu^2 < 0$  configuration the field breaks spontaneously the symmetry reaching the  
 641       ground state, acquiring an expectation value on vacuum different from zero,  $v$ .

### 642   2.2.3 Englert-Brout-Higgs mechanism

643     After the spontaneous symmetry breaking, the scalar doublet transforms into the form  
 644       given in equation 2.14, where  $G^+$  and  $G^0$  are the Goldstone bosons product of the break-  
 645       ing of the  $SU(2)$  symmetry, and  $H$  is the Englert-Brout-Higgs boson. From Goldstone’s,  
 646       theorem when a symmetry is spontaneously broken a massless boson appear for each

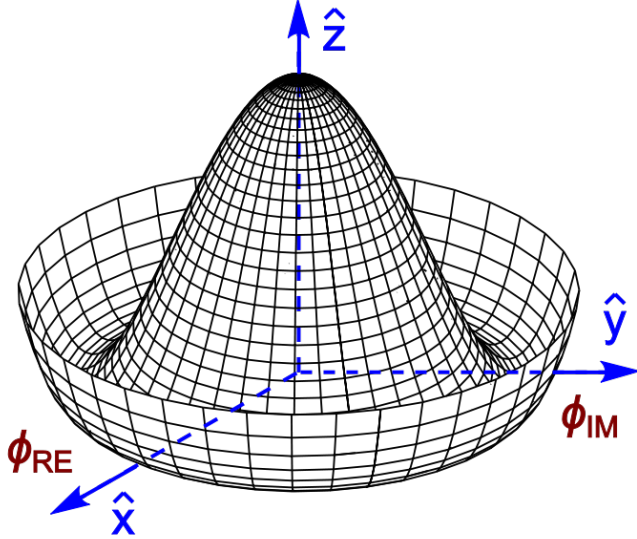


Figure 2.1: Higgs potential

broken generator. In our specific case, the three generators of  $SU(2)$  are broken giving rise to three Goldstone bosons:  $G^+$ ,  $G^-$  and  $G^0$ . This massless bosons are “eaten” by the  $W^+$ ,  $W^-$  and  $Z^0$  giving them an additional degree of freedom, the longitudinal polarization.

$$\Phi = \begin{pmatrix} G^+ \\ \frac{1}{\sqrt{2}}(H + v - iG^0) \end{pmatrix} \quad (2.14)$$

By this mechanism, the  $W$  and  $Z$  bosons acquire mass, being its value set by the coupling constant of  $SU(2)$  group and the vacuum expectation value of Englert-Brout-Higgs boson. In addition, the fermions on the theory also acquire a mass from the interactions with the scalar doublet. Such masses are in general of the form  $m_f = \lambda_f v / \sqrt{2}$ , where  $\lambda_f$  sets the interaction between the Englert-Brout-Higgs boson and the fermion. Finally, also the Englert-Brout-Higgs boson has a mass  $m_H^2 = -2\mu^2$ .

In summary, with this mechanism the weak interaction bosons and fermions of the theory are given a mass on the price of introducing an additional scalar field to spontaneously break the  $SU(2)$  symmetry.

### 2.3 Hierarchy problem and other limitations

The SM has been one of the most successful theories on the history of physics. With only 19 free parameters, is able to make thousands of predictions that have been measured and tested over the last seventy to eighty years. However some aspects in the model

are not completely understood. The most important one is the so-called hierarchy mass problem. At tree level, the Englert-Brout-Higgs boson has a mass  $m_H^2 = -2\mu^2$ , but the physical mass also contain the one-loop contributions from fermions that interact with it, as the top quark. The Feynman diagram for such contribution can be seen in figure 2.2.

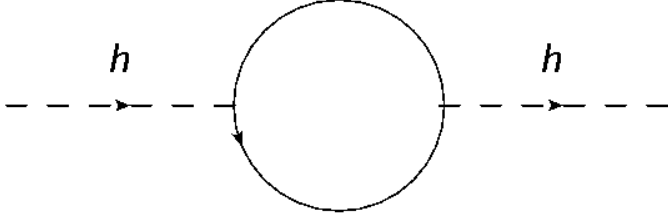


Figure 2.2: One loop diagram for contributions to the mass of the Englert-Brout-Higgs boson from interactions with fermions

Such contributions add up giving a mass greater than simple tree level mass. Each fermion contributes proportionally to its mass, what means that the top quark contributes the most. Moreover, if there are in nature heavier fermions that also interact with the Englert-Brout-Higgs boson they will also contribute to its mass. With such considerations one can expect the Englert-Brout-Higgs boson to be much greater than 125 GeV, and in principle not even of the order of 100 GeV but greater than 1 TeV. However the real relevance or significance of this problem at theoretical level has been discussed extensively, for example at [9], the majority of the community agrees there is something to be understood on the subject.

The most famous proposed solution to this problem is supersymmetry (SUSY) [10]. It proposes the existence of an additional symmetry between fermions and bosons, at a given point of the history of universe nature didn't distinguish between fermions and bosons. However, we know this does not happen at the present, and then this symmetry should be broken. Such symmetry implies the existence of a super-symmetric partner for each particle, a super-partner. A fermion for each boson and vice versa. This SUSY procedure doubles the particle content of the model where it's applied. Before breaking SUSY, a particle and its partner have the same mass. In this feature is where the hierarchy problem is solved. On figure 2.3 one can see the one loop diagrams for the mass of the Englert-Brout-Higgs boson from the top and its super-partner the stop. Whereas, the top contribution is positive, the stop contribution is negative but equal in value, then cancelling between them.

But this solution works exactly only if SUSY is not broken. As we know SUSY has to be broken, there has been developed in the literature different ways to brake SUSY and still offer a solution to the hierarchy problem, leading normally to solutions that need a fine adjustment of the parameters of the theory. This represents for some theoreticians a problem itself: Fine-tuning or Naturalness. Extensive searches for SUSY particles have been performed, accordingly to different model realizations MSSM [11, 12], CMSSM,

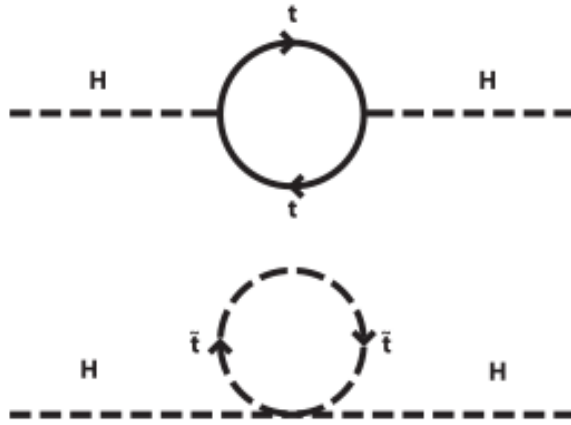


Figure 2.3: One loop diagrams for contributions to the mass of the Englert-Brout-Higgs boson from the top and the stop

696 etc.

697 While hierarchy problem is an internal problem of the SM, there are several questions  
 698 that have not been solved. For example, how gravity is understood in the frame of QFT's,  
 699 why there is only 3 generations of leptons and quarks, why there is only 4 fundamental  
 700 forces among others. In addition, there have been experimental questionings to the SM.  
 701 The mos important one is the masses of neutrinos. In the SM neutrinos are massless,  
 702 careful measurements, [13, 14], have shown that neutrinos can oscillate between different  
 703 flavors, phenomenon only possible if neutrinos have a mass. Measurements of solar and  
 704 atmospheric neutrino oscillations have been the most important proof of physics beyond  
 705 the SM.

706 From cosmological measurements, the Wilkinson Microwave Anisotropy Probe have  
 707 shown that the universe is not only made by visible matter, but suggests that around  
 708 24% its made of dark matter. A type of matter not visible by means of light. It has also  
 709 shown that 71% of the universe is composed of dark energy, what makes the universe to  
 710 be in an accelerated state of expansion. These results can be seen in [15, 16]. Also the  
 711 Planck probe has shown similar results, for example in [17]. The SM does not have any  
 712 answer to this open problems so far.

713 Finally, there is known that the universe presents an asymmetry between matter  
 714 and antimatter, being the first much more abundant than the second. Such asymmetry  
 715 can be obtained by CP-violating processes (C for charge and P for parity). However  
 716 the amount of CP violation present in the SM is not compatible with the huge matter-  
 717 antimatter asymmetry in nature. This problem, known as baryon asymmetry, represent  
 718 an additional huge challenge for particle physics.

719 In conclusion, the SM has been a formidable model that has helped us to understand

720 a huge amount of physics. It has done thousands of predictions that have been measured  
721 and corroborated one by one in the last half-century. However, this is not the end of the  
722 story, perhaps only the beginning. There are theoretical and experimental motivations  
723 that lead us think that the SM is not the “final” theory that could explain all subatomic  
724 phenomena in nature. Currently, there is a mayor effort, both theoretical and experi-  
725 mentally, to understand and explain all the remaining pieces. The present work is one  
726 of them.

727 In the next chapter, we present an extension of the SM that looks for a solution to  
728 the discussed hierarchy problem.



729 **Chapter 3**

730 **Vector Like Quarks: Generic  
model**  
731

732 From chapter 2 we have seen how there are some parts in the SM that does not work very  
733 well. From such internal issues some further models/theories have been developed. All  
734 this theories are commonly grouped under the term Beyond Standard Model or simply  
735 BSM. One of the most famous BSM theory is supersymmetry (SUSY). This theory  
736 postulates a symmetry that does not distinguish between fermions and bosons. This  
737 idea have given birth to a plethora of model realizations and physics predictions. So far,  
738 nothing of the new consequences of this theory have been confirmed but the experiments  
739 have an enormous investment on their search. But not only SUSY have seen the day  
740 light, there is on the market an astonishing amount of BSM theories addressing different  
741 issues of the SM. Extra dimensions, fourth families, composite Higgs are a few of them.

742 In this chapter we will describe a bunch of models that introduce additional heavy  
743 quarks, heavier than the top, in order to solve the hierarchy problem, described on  
744 section 2.3.

745 **3.1 Motivation**

746 **3.2 Generic Formulation**

747 **3.3 Fesability study for a search of a  $T$  at LHC at 8 TeV**

748 **3.3.1 Production modes**

749 **3.3.2 Decay modes**

750 **3.3.3 Stragey for the full hadronic final state**

751 **3.3.4 Event selection**

752 **3.3.5 Results**



753 **Chapter 4**

754 **Understanding theory predictions  
755 via Monte-Carlo event generation**

756 Although we have nowadays a very elegant and complete theoretical description of par-  
757 ticle physics, is not always evident how to translate this theory in actual predictions, to  
758 compare with measurements. Moreover, on the case of hadronic colliders, as the LHC,  
759 it's even more difficult due to the particularities of strong interaction. On this subject,  
760 a set of tools and approaches have been developed in order to be able to make accurate  
761 predictions from theory that could be directly researched for on the experiments, as CMS  
762 or ATLAS for example. In the present chapter, we describe such tools and formalisms  
763 and a set of studies comparing the predictions these tools to data.

764 **4.1 Mote-Carlo simulations**

765 The Monte-Carlo simulations use random numbers and large samplings to calculate  
766 mathematical quantities in complex configurations, as integrals or probabilities. The  
767 typical example is on how to calculate the integral of a one-dimensional function. One  
768 can throw several random coordinates pair in the Cartesian plane and count how many  
769 of them are under the function. Then the integral of the function will be proportional  
770 to the fraction of points under the curve to the total thrown points. Larger the number  
771 of points, closer the estimation to the real value. An illustration of the procedure can  
772 be seen in figure 4.1.

773 A similar method is used to simulate proton-proton collisions. This simulation is  
774 used to generate “random” events and to calculate quantities, as the cross section, for a  
775 given physical process. Each event represent the final state of a collision, i.e. the set of  
776 particles produced from the collision and seen by a detector. Such simulations compre-  
777 hend different stages: first, the partonic processes making reference to the interaction  
778 between the partons inside the proton; second, the hadronization of the particles pro-  
779 duce from parton interactions; and third, the simulation of the interaction between the  
780 hadrons (from second step) and the detector material. Such events are used to evaluate  
781 predictions from theory in the frame of a specific experiment. Whereas the hadronization

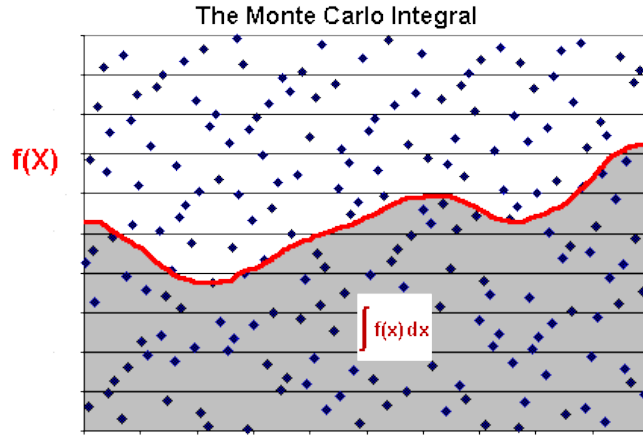


Figure 4.1: Integration using Monte-Carlo methods

782 and detector simulation are well-known physical processes, new theories predictions rely  
 783 basically on the partonic part, where the fundamental interaction processes take part

#### 784 4.1.1 Parton simulation

785 The parton model was initially proposed by Richard Feynman in 1969, as a method to un-  
 786 derstand collisions of non-fundamental particles. The model consider a non-fundamental  
 787 particle, as a proton or a neutron, composed of a given number of point-like fundamental  
 788 particles. When a collision occur the point-like particles inside have a major probability  
 789 to scatter. For example, when an electron is fired against a proton the most of the  
 790 interactions will between the electron and the fundamental components of the proton,  
 791 *u* and *d* quarks. This “hard” components are called *valence* quarks. Surrounding them  
 792 there are the *sea* quarks and gluons.

793 However, as the energy of the collision increases the probability to scatter a sea  
 794 component, quark or gluon, increases.

795 **4.1.2 Hadron simulation**

796 **4.1.3 Detector simulation**

797 **4.2 Tools**

798 **4.2.1 Matrix-element generators**

799 **4.2.2 Hadron generators**

800 **4.2.3 Detector simulation**

801 **4.3 Validation on data**



802 **Chapter 5**

803 **Search for a single produced T'**  
804 **decaying into top and Higgs in**  
805 **the full hadronic final state**

806 In the present chapter we describe in full detail the search performed using 2012 data  
807 collected by CMS for a T' in the full hadronic final state. The theoretical formalism for  
808 such object has been described on chapter 3.

809 **5.1 Analysis Strategy**

810 **5.2 Datasets**

811 **5.3 Event selection**

812 **5.3.1 T' reconstruction with a  $\chi^2$  sorting algorithm**

813 **5.3.2 Efficiencies**

814 **Trigger**

815 **Selection**

816 **5.4 Background estimation from data**

817 **5.4.1 Known difficulties and tried methods**

818 **5.4.2 Method**

819 **5.4.3 Validation**

820 **5.5 Systematics**

821 **5.6 Results**

## <sup>822</sup> Bibliography

- <sup>823</sup> [1] O. S. Brüning, P. Collier, P. Lebrun, S. Myers, R. Ostojic, J. Poole, and  
<sup>824</sup> P. Proudlock, *LHC Design Report*. CERN, Geneva, 2004.
- <sup>825</sup> [2] **CMS Collaboration** Collaboration, G. L. Bayatian *et al.*, *CMS Physics: Technical Design Report Volume 1: Detector Performance and Software*. Technical Design Report CMS. CERN, Geneva, 2006. There is an error on cover due to a technical problem for some items.
- <sup>829</sup> [3] **CMS Collaboration** Collaboration, G. L. Bayatian *et al.*, “CMS Physics: Technical Design Report Volume 2: Physics Performance,” *J. Phys. G* **34** no. CERN-LHCC-2006-021. CMS-TDR-8-2, (2007) 995–1579. 669 p. revised version submitted on 2006-09-22 17:44:47.
- <sup>833</sup> [4] **ATLAS Collaboration** Collaboration, A. Collaboration, *ATLAS detector and physics performance: Technical Design Report*. Technical Design Report ATLAS. CERN, Geneva, 1999. Electronic version not available.
- <sup>836</sup> [5] **LHCb Collaboration** Collaboration, J. Alves, A. Augusto *et al.*, “The LHCb Detector at the LHC,” *JINST* **3** (2008) S08005.
- <sup>838</sup> [6] **ALICE Collaboration** Collaboration, P. Cortese, C. W. Fabjan, L. Riccati, K. Safarík, and H. de Groot, *ALICE physics performance: Technical Design Report*. Technical Design Report ALICE. CERN, Geneva, 2005. revised version submitted on 2006-05-29 15:15:40.
- <sup>842</sup> [7] **UA4/2 Collaboration** Collaboration, C. Augier *et al.*, “Predictions on the total cross-section and real part at LHC and SSC,” *Phys.Lett.* **B315** (1993) 503–506.
- <sup>844</sup> [8] C. Mathis, T. Bhattacharya, and S. Imari Walker, “The Emergence of Life as a First Order Phase Transition,” *ArXiv e-prints* (Mar., 2015) , [arXiv:1503.02776](https://arxiv.org/abs/1503.02776) [[nlin.AO](#)].
- <sup>847</sup> [9] F. Jegerlehner, “The hierarchy problem of the electroweak Standard Model revisited,” [arXiv:1305.6652](https://arxiv.org/abs/1305.6652) [[hep-ph](#)].
- <sup>849</sup> [10] S. P. Martin, “A Supersymmetry primer,” *Adv.Ser.Direct.High Energy Phys.* **21** (2010) 1–153, [arXiv:hep-ph/9709356](https://arxiv.org/abs/hep-ph/9709356) [[hep-ph](#)].

- 851 [11] **CMS** Collaboration, V. Khachatryan *et al.*, “Search for neutral MSSM Higgs  
852 bosons decaying to a pair of tau leptons in pp collisions,” *JHEP* **1410** (2014) 160,  
853 [arXiv:1408.3316](https://arxiv.org/abs/1408.3316) [hep-ex].
- 854 [12] **ATLAS** Collaboration, G. Aad *et al.*, “Search for neutral Higgs bosons of the  
855 minimal supersymmetric standard model in pp collisions at  $\sqrt{s} = 8$  TeV with the  
856 ATLAS detector,” *JHEP* **1411** (2014) 056, [arXiv:1409.6064](https://arxiv.org/abs/1409.6064) [hep-ex].
- 857 [13] **Super-Kamiokande** Collaboration, Y. Ashie *et al.*, “Evidence for an oscillatory  
858 signature in atmospheric neutrino oscillation,” *Phys.Rev.Lett.* **93** (2004) 101801,  
859 [arXiv:hep-ex/0404034](https://arxiv.org/abs/hep-ex/0404034) [hep-ex].
- 860 [14] C. Weinheimer and K. Zuber, “Neutrino Masses,” *Annalen Phys.* **525** no. 8-9,  
861 (2013) 565–575, [arXiv:1307.3518](https://arxiv.org/abs/1307.3518).
- 862 [15] C. L. Bennett, D. Larson, J. L. Weiland, N. Jarosik, G. Hinshaw, N. Odegard,  
863 K. M. Smith, R. S. Hill, B. Gold, M. Halpern, E. Komatsu, M. R. Nolta, L. Page,  
864 D. N. Spergel, E. Wollack, J. Dunkley, A. Kogut, M. Limon, S. S. Meyer, G. S.  
865 Tucker, and E. L. Wright, “Nine-year Wilkinson Microwave Anisotropy Probe  
866 (WMAP) Observations: Final Maps and Results,” *The Astrophysical Journal,*  
867 *Supplement* **208** (Oct., 2013) 20, [arXiv:1212.5225](https://arxiv.org/abs/1212.5225) [astro-ph.CO].
- 868 [16] G. Hinshaw, D. Larson, E. Komatsu, D. N. Spergel, C. L. Bennett, J. Dunkley,  
869 M. R. Nolta, M. Halpern, R. S. Hill, N. Odegard, L. Page, K. M. Smith, J. L.  
870 Weiland, B. Gold, N. Jarosik, A. Kogut, M. Limon, S. S. Meyer, G. S. Tucker,  
871 E. Wollack, and E. L. Wright, “Nine-year Wilkinson Microwave Anisotropy Probe  
872 (WMAP) Observations: Cosmological Parameter Results,” *The Astrophysical  
873 Journal, Supplement* **208** (Oct., 2013) 19, [arXiv:1212.5226](https://arxiv.org/abs/1212.5226) [astro-ph.CO].
- 874 [17] **Planck** Collaboration, P. Ade *et al.*, “Planck 2015 results. XIII. Cosmological  
875 parameters,” [arXiv:1502.01589](https://arxiv.org/abs/1502.01589) [astro-ph.CO].

# 876 Contents

|     |  |           |
|-----|--|-----------|
| 877 | <b>1 The CMS experiment at LHC</b>                                   | <b>3</b>  |
| 878 | 1.1 The Large Hadron Collider . . . . .                              | 3         |
| 879 | 1.1.1 Injector chain . . . . .                                       | 4         |
| 880 | 1.1.2 Main ring . . . . .  | 6         |
| 881 | 1.1.3 Run 1 . . . . .  | 9         |
| 882 | 1.1.4 Other experiments at LHC . . . . .                             | 10        |
| 883 | 1.2 The Compact Muon Solenoid experiment . . . . .                   | 13        |
| 884 | 1.2.1 Coordinate system . . . . .                                    | 13        |
| 885 | 1.2.2 Magnet . . . . .   | 17        |
| 886 | 1.2.3 Tracker system . . . . .                                       | 17        |
| 887 | 1.2.4 Electromagnetic calorimeter . . . . .                          | 18        |
| 888 | 1.2.5 Hadronic Calorimeter . . . . .                                 | 20        |
| 889 | 1.2.6 Muon chambers . . . . .  | 22        |
| 890 | 1.2.7 Trigger . . . . .  | 22        |
| 891 | <b>2 The Standard Model</b>  | <b>27</b> |
| 892 | 2.1 Fields, symmetries and interactions . . . . .                    | 28        |
| 893 | 2.2 Quantum fields and particles . . . . .                           | 30        |
| 894 | 2.2.1 The mass problem . . . . .                                     | 32        |
| 895 | 2.2.2 Spontaneous Symmetry Breaking . . . . .                        | 33        |
| 896 | 2.2.3 Englert-Brout-Higgs mechanism . . . . .                        | 33        |
| 897 | 2.3 Hierarchy problem and other limitations . . . . .                | 34        |
| 898 | <b>3 VLQ models</b>  | <b>39</b> |
| 899 | 3.1 Motivation . . . . .   | 39        |
| 900 | 3.2 Generic Formulation . . . . .                                    | 39        |
| 901 | 3.3 Fesability study for a search of a $T$ at LHC at 8 TeV . . . . . | 39        |
| 902 | 3.3.1 Production modes . . . . .                                     | 39        |
| 903 | 3.3.2 Decay modes . . . . .  | 39        |
| 904 | 3.3.3 Stragey for the full hadronic final state . . . . .            | 39        |
| 905 | 3.3.4 Event selection . . . . .                                      | 39        |
| 906 | 3.3.5 Results . . . . .  | 39        |

|     |   |           |
|-----|---|-----------|
| 907 | <b>4 MC event generation</b>  | <b>41</b> |
| 908 | 4.1 Mote-Carlo simulations . . . . .                                  | 41        |
| 909 | 4.1.1 Parton simulation . . . . .                                     | 42        |
| 910 | 4.1.2 Hadron simulation . . . . .                                     | 43        |
| 911 | 4.1.3 Detector simulation . . . . .                                   | 43        |
| 912 | 4.2 Tools . . . . .   | 43        |
| 913 | 4.2.1 Matrix-element generators . . . . .                             | 43        |
| 914 | 4.2.2 Hadron generators . . . . .                                     | 43        |
| 915 | 4.2.3 Detector simulation . . . . .                                   | 43        |
| 916 | 4.3 Validation on data . . . . .                                      | 43        |
| 917 | <b>5 Single VLQ search</b>  | <b>45</b> |
| 918 | 5.1 Analysis Strategy . . . . .                                       | 46        |
| 919 | 5.2 Datasets . . . . .  | 46        |
| 920 | 5.3 Event selection . . . . .   | 46        |
| 921 | 5.3.1 $T'$ reconstruction with a $\chi^2$ sorting algorithm . . . . . | 46        |
| 922 | 5.3.2 Efficiencies . . . . .  | 46        |
| 923 | 5.4 Background estimation from data . . . . .                         | 46        |
| 924 | 5.4.1 Known difficulties and tried methods . . . . .                  | 46        |
| 925 | 5.4.2 Method . . . . .  | 46        |
| 926 | 5.4.3 Validation . . . . .  | 46        |
| 927 | 5.5 Systematics . . . . .   | 46        |
| 928 | 5.6 Results . . . . .   | 46        |